universität wien

MASTERARBEIT / MASTER'S THESIS

Titel der Masterarbeit / Title of the Master's Thesis

„Curing cancer in dogs: Generation of caninized checkpoint inhibitors anti-PD-1 and anti-PD-L1 mAbs with specific canine constant IgG1 and IgG4 domains"

verfasst von / submitted by

Nicoletta Marquardt, BSc

angestrebter akademischer Grad / in partial fulfilment of the requirements for the degree of

Master of Science (MSc)

Wien, 2022 / Vienna, 2022

Studienkennzahl lt. Studienblatt / degree programme code as it appears on the student record sheet:	UA 066 834
Studienrichtung lt. Studienblatt / degree programme as it appears on the student record sheet:	Master's degree programme Molecular Biology
Betreut von / Supervisor:	Univ.-Prof. Dr. med. Erika Jensen-Jarolim

Declaration of Authorship

I hereby declare that this Master Thesis has been written by myself and that I have not previously submitted this work in any form either in Austria or abroad. I have not used any other than the listed sources, nor have I received any unauthorized help. Furthermore, I assure that the printed and electronic copies I have submitted are identical.

Date: Signature:

Acknowledgements

I would like to thank my supervisor, Univ. Prof. Dr. med. Erika Jensen-Jarolim, for her dedicated support and opportunities I was given during the whole master project. Her valuable input led to constructive discussions and new ideas throughout the process.

Furthermore, I want to deeply thank my Co-supervisor Rodolfo Bianchini, PhD, for his invaluable support, always taking his time for discussing arising issues together, leading to interesting new ideas throughout the whole project. I would like to thank him for his patience and helpful scientific advice, as well as his inspiring and positive attitude.

Thank you also to Mira Matz, MSc, for all her technical input and interesting advice.

Also, I would like to thank Gerlinde Hofstetter, MSc., for her expertise, answering numerous questions concerning methodology and general issues in the lab.

I want to thank the whole Messerli team for the awesome working atmosphere, it was a pleasure working together with all of them, leading to invaluable new friendships. A special thanks to Hanna Mayerhofer, MSc., who supported me not only mentally, but also with her scientific expertise. Finally, a big thanks to my family and friends, for always supporting me and being there for me.

Abstract

Background: To date, the most successful human anti-cancer immunotherapies include monoclonal antibodies (mAbs) against the checkpoint molecule programmed cell death protein 1 (PD-1) and its ligand programmed death-ligand 1 (PD-L1), while the development of equivalent anti-cancer immunotherapies for dogs (canine cancer; *Canis familiaris*) lags far behind. To overcome this limitation, the goal of this project was the generation of caninized anti-PD-1 and anti-PD-L1 mAbs with canine IgG1 or IgG4 constant regions.

Methods: Plasmid production in *Escherichia coli* was optimized, followed by purification and DNA sequencing. Eukaryotic Expi293F cells were transfected and mAbs were purified via affinity chromatography. SDS-PAGE, western blots and dot blots were used to detect caninized mAbs. Flow cytometric analyses were undertaken to determine the binding capacities of human anti-PD-1 and anti-PD-L1 mAbs to canine cancer cell lines, as well as to the expression cell line Expi293F.

Results: Via dot blots, mAbs of all isotypes were detected in the cell culture of transfected Expi293F cells. On SDS-PAGE and western blots, purified caninized IgG1 anti-PD-L1 mAbs showed one band at a size of 150 kDa under non-reducing conditions corresponding to full-length antibodies and two bands with sizes of 50 kDa and 25 kDa, under reducing conditions, corresponding to heavy and light chains. Results from flow cytometric analyses showed significant binding of human anti-PD-1 and anti-PD-L1 mAbs to all the canine cancer cell lines, however also to the expression cell line Expi293F.

Conclusions: Overall, the results of our study provide an important foundation towards the establishment of an immunotherapy against dog cancer.

Kurzzusammenfassung

Hintergrund: Zu den am häufigsten angewandten Immuntherapien für die Behandlung von Krebs beim Menschen gehören monoklonale Antikörper (mAK), welche das Checkpoint-Molekül „programmed cell death protein 1“ (PD-1) und deren Liganden, „programmed death-ligand 1“ (PD-L1), hemmen. Vergleichbare Therapien sind für die Behandlung von Krebs bei Hunden (caniner Krebs; *Canis familiaris*) nicht verfügbar. Das Ziel dieses Projekts war deshalb die Entwicklung caninisierter anti-PD-1 und anti-PD-L1 mAK, mit spezifischem caninen IgG1 oder IgG4.

Methoden: Die Produktion von Plasmiden in *Escherichia coli* wurde optimiert, gefolgt von DNA-Aufreinigung und Sequenzierung. Eukaryotische Expi293F Zellen wurden transfektiert und mAK wurden mithilfe von Affinitätschromatographie aufgereinigt. SDS-PAGE, Western blots und Dot blots wurden zur Detektion der caninisierten mAK angewandt. Durchflusszytometrie wurde verwendet, um Bindungsaffinitäten von humanen anti-PD-1 und anti-PD-L1 mAK zu caninen Krebszelllinien, als auch zur Expressionszelllinie Expi293F, festzustellen.

Ergebnisse: Mithilfe von Dot Blots wurden mAK aller Isotypen in der Zellkultur transfizierter Expi293F Zellen detektiert. Aufgereinigte caninisierte anti-PD-L1 IgG1 mAK wiesen auf SDS-PAGE und Western Blots unter nicht reduzierenden Bedingungen eine Proteinbande mit einer Größe von 150 kDa auf, welche der Gesamtgröße des mAK entspricht, während unter reduzierenden Bedingungen zwei Proteinbanden mit Größen von 50 kDa und 25 kDa detektiert wurden, entsprechend den schweren und leichten Ketten der Antikörper. Ergebnisse der Durchflusszytometrie wiesen signifikante Bindungsaffinitäten der humanen anti-PD-1 und anti-PD-L1 mAK zu den caninen Krebszelllinien auf, jedoch ebenso zur Expressionszelllinie Expi293F.

Schlussfolgerung: Zusammenfassend bereiten die Resultate unserer Studie wichtige Grundlagen für die Entwicklung einer Immuntherapie gegen Krebs bei Hunden.

List of abbreviations

APC	Allophycocyanin
APC	Antigen presenting cell
bp	Base pair
CHO cell	Chinese hamster ovary cell
CMV	Cytomegalovirus
CV	Column volume
DC	Dendritic cell
DMEM	Dulbecco's Modified Eagle's Medium
DNA	Deoxyribonucleic acid
E. coli	*Escherichia coli*
EF-1α	Elongation factor 1 alpha
ÊGFR	Epidermal growth factor receptor
FBS	Fetal bovine serum
FDA	United States Food and Drug Administration
FMDV	Foot and Mouth Disease Virus
GM-CSF	Granulocyte-macrophage colony-stimulating factor
HRP	Horseradish peroxidase
ICI	Immune checkpoint inhibitor
IFN-α/ -β/ -γ	Interferon-alpha/ -beta /-gamma
IgG	Immunoglobulin
IL-2	Interleukin-2
IRES	Internal ribosome entry site
LB	Lysogeny Broth
mAb	Monoclonal antibody
MFI	Mean fluorescent intensity
MOE-PCR	Multiple overlap extension polymerase chain reaction
NK cell	Natural killer cell
OD_{600}	Optical density at a wavelength of 600 nm
pAn	polyadenylation signal
PBS	Phosphate-buffered saline
PD-1	Programmed cell death protein 1
PD-L1	Programmed death-ligand 1

RT	Room temperature
SDS-PAGE	Sodium dodecyl sulfate polyacrylamide gel electrophoresis
SV40	Simian virus 40
TAM	tumor-associated macrophages
TB	Terrific Broth
TBS-T	Tris-buffered saline with tween
Th-1 cell	T helper 1 cell
TME	Tumor microenvironment
TNF-α	Tumor necrosis factor alpha
Treg	T regulatory cell

Table of Content

1. Introduction

1.1. Cancer in human

Cancer is among the leading causes of death worldwide, with approximately 19 million new cases in 2020, accounting for 10 million deaths (Sung et al., 2021). The most common types of cancer leading to death in 2020 were lung, colon and rectum, liver, stomach and breast cancer (WHO, 2022). However, the prevalence of certain cancer types varies between countries, depending on the degree of economic development as well as social and environmental factors. In high-income countries, cancer development is frequently associated with Western lifestyle choices, including tobacco use, alcohol consumption, diet, obesity and lack of physical activity. Overall, those countries have the highest incidence of all cancer cases, while mortality rates are declining due to prevention strategies as well as the availability of successful treatments. In low-income countries on the other hand, cancer-related mortality remains high (Hulvat, 2020), with cancer-causing infections such as human papillomavirus accounting for 30 % of cancer cases (WHO, 2022). Cancer, also termed malignant tumor or neoplasm, summarizes a large group of more than 100 diseases that can affect any part of the body. It is characterized by uncontrollable growth of mutated cells, which escape their usual metabolic growth control mechanisms and in later stages of disease invade adjoining tissues and spread to other organs, which is referred to as metastasis (Gonzalez et al., 2018). The major cause of death from solid tumors is due to metastasis (Seyfried et al., 2013), (Dillekås et al., 2019). Conversion of normal cells into malignant cells occurs in a multi-stage process characterized by genetic instability, escape of immunosurveillance and tumor cell heterogeneity (Pérez-Herrero et al., 2015). A row of mechanisms involved in tumorigenesis were proposed by Hanahan and Weinberg in 2000 and updated over the years, providing a framework in understanding the process of tumorigenesis (*figure 1*). The so-called hallmarks of cancer include sustained proliferative signaling, evasion of growth suppressors, enabling replicative immortality, resisting cell death, induced angiogenesis, activating invasion and metastasis, avoiding immune destruction, and deregulating cellular metabolism. Acquisition of these characteristics is considered to require i) Genomic instability leading to random mutations and ii) tumor-promoting inflammation (Hanahan et al., 2011).

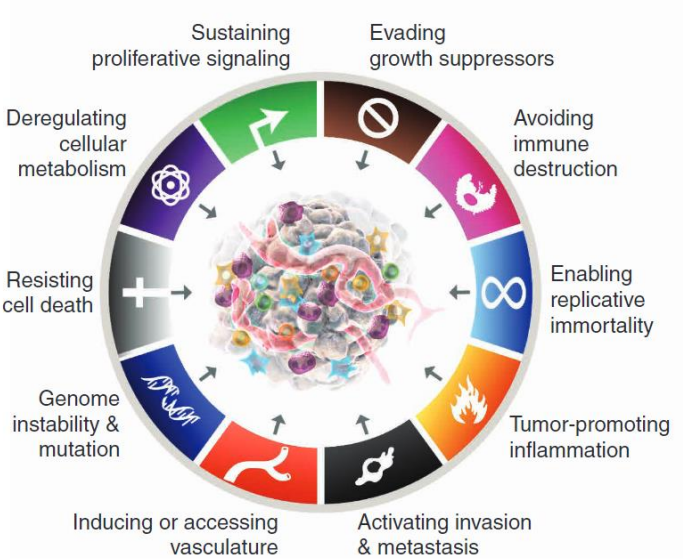

figure 1: The hallmarks of cancer propose a network of acquired mechanisms driving the progression of tumorigenesis (Hanahan, 2022).

The proposed characteristics, especially the tight contact with blood-born immune cells, highlight the critical role of the immune system in either prevention but also progression of tumor pathogenesis. For development of treatment strategies, is essential to understand the hallmarks as codependent network instead of individual segregated processes (Fouad et al., 2017).

1.2. Immune system involved in cancer

The immune system plays a double-edged role in tumor pathogenesis. In early stages of tumor development, immune cells sense and destroy mutated potentially malignant cells, while in later stages, the immune system unfortunately most often promotes tumor progression (Schreiber et al., 2011). In this respect, evolution of a highly specialized tumor microenvironment (TME) plays a major role in malignant tumor development. The function of tumor-infiltrated immune cells in the TME is suppressed by multiple mechanisms leading to impairment of the immune recognition of tumor cells and enhanced inflammation, promoting tumorigenesis (Wei et al., 2021). The immunoediting hypothesis, consisting of 3 phases: elimination, equilibrium and escape, see figure 2, describes the dynamic process of immune modulation during tumor progression. The first phase, elimination, refers to the stage of active immune surveillance, whereat the innate and adaptive branches of the immune system work together to recognize and eliminate potentially malignant cells. Cells have the potential of becoming malignant when genetic mutations are not repaired by the regular DNA repair mechanisms. Mutated cells are recognized by the immune system via detection of biochemical differences (Abbott et al., 2019) and destroyed by cytotoxic immune cells. Cancer cell variants

that are less immunogenic might escape elimination, leading to the phase of equilibrium (Gonzalez et al., 2018), whereat tumor cells enter a dormant stage and continue to coexist with the immune system. This phase can take up to years. Eventually, dormant tumor cells escape immune regulation and start proliferating in a non-restricted manner, leading to rapid cell growth and clinically visible tumors (Muenst et al., 2016). Malignant cells escape immune surveillance by a row of different mechanisms, leading to suppression of immune cells, resistance to immune attack mechanisms and creation of an immunomodulating TME (Abbott et al., 2019).

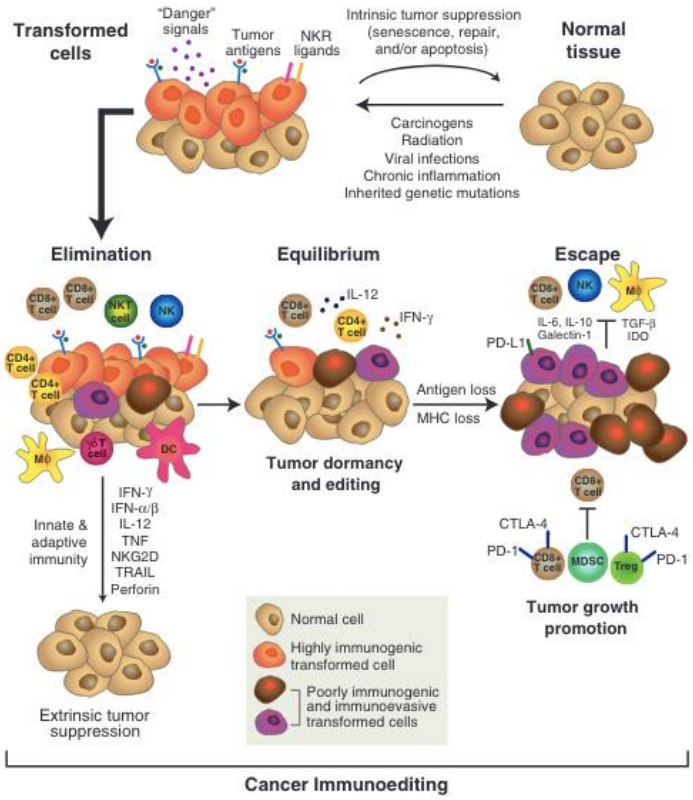

figure 2: The cancer immunoediting hypothesis describes the dynamic process of immune modulation in tumorigenesis, consisting of three phases: elimination, equilibrium and escape. Various factors lead to malignant transformation of normal cells, which are then recognized by immune cells and destroyed (Elimination). Less immunogenic tumor cells remain undetected from the immune system (Equilibrium). Transformed cells develop mechanisms to evade immune evasion and proliferate in a non-restricted manner (Escape) (Abbott et al., 2019).

T lymphocytes, including regulatory T cells (Tregs), cytotoxic T cells ($CD8^+$ cells) and helper T cells ($CD4^+$ cells), play a critical role in antitumor immunosurveillance. In the early stages of tumorigenesis, upon activation by antigen presenting cells (APCs) such as dendritic cells (DCs), $CD8^+$ T lymphocytes differentiate into cytotoxic T cells and eliminate tumor cells. The $CD4^+$ T helper 1 cells (Th-1 cells) express proinflammatory cytokines, such as Tumor necrosis factor alpha (TNF-α), Interleukin-2 (IL-2) and Interferon-gamma (INF-γ), leading to activation of macrophages, natural killer (NK) cells, and increased $CD8^+$ T cell activation. The presence

of high numbers of cytotoxic T cells as well as Th-1 cells in the TME correlates with a favorable cancer prognosis (Gonzalez et al., 2018). However, upon tumor progression, cancer cells modulate the microenvironment via various pathways, leading to a decrease in antigen-presentation on APCs, reduced cytotoxic T cell differentiation, down-regulation of Th-1 anti-tumor response and an increase in Tregs and tumor-associated macrophages (TAMs) (Kim et al., 2022). Tregs block anti-tumor functions via secretion of inhibitory cytokines into the TME, suppressing cytotoxic $CD8^+$ T lymphocytes, Th-1 cells, NK cells, B cells and APCs (Muenst et al., 2016). TAMs in the TME account for 50 % of all immune cells, promoting cancer progression via supplement of nutrients to cancer cells (Kim et al., 2022) and checkpoint molecule expression, blocking cytotoxic T cell responses. TAMs correlate with the pro-tumor M2 macrophage phenotype and develop from newly recruited monocytes as well as macrophages resident in a certain tissue due to certain factors upregulated in the TME such as cytokines and chemokines (Brom et al., 2022).

1.3. Human cancer treatments

Over the past decades, there has been a shift in human cancer therapy from conservative treatments such as surgery, radiotherapy and chemotherapy to targeted treatments. Among them, cancer immunotherapies particularly aim at exploiting the immune system against cancer-specific molecules with a key role in proliferation, or indirectly at blocking the immunosuppressive function of infiltrating immune cells. For the treatment of local solid tumors, surgery and radiotherapy are mainly effective, however ineffective upon tumor metastasis. Chemotherapy is based on the toxicity of administered drugs, which inhibit division of rapidly proliferating cells, targeting cancer cells but also normal cells with high proliferation rate such as hair follicles, bone marrow and gastrointestinal tract cells, leading to side effects. (Pérez-Herrero et al., 2015). Chemotherapy and radiotherapy, summarized as conservative cancer treatment, exhibit several drawbacks, including lack of specificity for targeting tumor cells, recurrence of drug-resistant tumors and systemic toxicity, highlighting the need for the development of novel therapies (Sanghera and Sanghera, 2019). Targeted cancer treatments aim to inhibit cancer cell proliferation via blocking specific molecular patterns or pathways utilized by tumor cells. These therapies either induce apoptosis of cancer cells, target and inhibit molecular signals in the TME leading to enhanced proliferation, direct chemotherapeutic agents to malignant cells or specifically restore the immune system function (Pérez-Herrero et al., 2015). Cancer immunotherapies include a variety of treatments that aim to stimulate the immune system to attack and destroy cancer cells. Antitumor immune responses are thus reactivated to overcome molecular pathways utilized by malignant cells. The main approaches of cancer immunotherapies include adoptive cell therapy, cytokine therapy, oncolytic viruses, cancer vaccines and immune checkpoint inhibitors (ICIs). (Kennedy et al., 2020). ICIs have

achieved notable clinical benefit in the treatment of various cancer types, such as non-small cell lung cancer, malignant melanoma, renal and bladder cancer (Brom et al., 2022). Particularly successful are monoclonal antibodies (mAbs) blocking interactions between programmed cell death protein 1 (PD-1), a co-inhibitory receptor highly expressed on tumor-specific activated T lymphocytes, and its ligand programmed death-ligand 1 (PD-L1), highly expressed on tumor cells (Sanghera et al., 2019).

1.4. Checkpoint molecule PD-1 and its ligand PD-L1

Immune checkpoint molecules are regulators of the immune system, exerting inhibitory or stimulatory effects on immune responses upon interaction with their ligands. Checkpoint molecules are expressed on cells of the immune system, and they are critical in the regulation of immune responses, modulating duration and magnitude of action and further prevent autoimmunity (Zhang et al, 2020). PD-1 is an immune checkpoint receptor, mainly expressed on activated T cells but also found on B cells, NK cells, monocytes, macrophages, DCs and Tregs, interacting with the ligands PD-1 and PD-L2 (Han et al., 2020). PD-L1 is expressed at low levels on APCs such as DCs, macrophages, mast cells, T and B cells as well as a variety of non-hematopoietic cells. PD-L2 expression is restricted to professional APCs including macrophages, DCs and B cells. Both ligands are expressed particularly under inflammatory conditions. PD-1 as well as its ligands are transmembrane proteins of the immunoglobulin (Ig) superfamily (Ai et al., 2020). Engagement between PD-1 on T cells and its ligands PD-L1 or PD-L2 inhibits T cell expansion, cytotoxic activity, and cytokine release. This checkpoint is essential for the regulation of T cell activity, limiting tissue damage during immune response (Plesca et al., 2020), and preventing autoimmune reactions.

However, cancer cells utilize this inhibitory mechanism by expressing high levels of PD-L1 on their surface, interacting with PD-1 expressed on T cells (Ai et al., 2020). Furthermore, inhibitory interactions were found between PD-L1 and CD80 (B7-1), expressed on APCs but also on T cells, inducing a reduction in T cell proliferation (Butte et al., 2007), (Plesca et al., 2020). TAMs also produce high levels of PD-L1 and PD-L2 on their surface, promoting immune suppression (Brom et al., 2022). Expression of PD-L1 is induced by pro-inflammatory cytokines, mainly by IFN-γ, while PD-L2 expression is upregulated by cytokines such as IL-4 and granulocyte-macrophage colony-stimulating factor (GM-CSF) (Plesca et al., 2020). PD-L2 receptor expression on tumor cells contributes immune evasion, however, PD-1/PD-L1 pathway is considered to be used more prominently by tumor cells (Ai et al., 2020). Anti-PD-1 and anti-PD-L1 mAbs aim to block interactions between the PD-1 receptor and its ligand PD-L1, having become a major cancer therapeutic strategy. By interfering with the inhibitory interaction between PD-1 and its ligand, cytotoxic T cell ability is restored, leading to killing of

tumor cells, as visualized in figure 3 (Eno, 2017). Further, checkpoint inhibition was shown to alter macrophage polarity from a pro-tumor M2 phenotype, associated with immunosuppression and impaired phagocytosis, towards the M1 phenotype, characterized by cytotoxic inflammatory conditions and restorage of phagocytic ability (Brom et al., 2022). MAbs targeting either PD-1 or PD-L1 are approved for the treatment of various human cancers, including melanoma, gastric and ovarian cancer, small cell and non-small cell lung cancer, renal cell carcinoma, head and neck squamous cell carcinoma and Hodgkin lymphoma (Kennedy et al., 2020). The mAb Pembrolizumab (= Keytruda), a PD-1 inhibitor was approved by the United States Food and Drug Administration (FDA) in 2014 (Eno, 2017), and by the European Commission in 2015 (EMA 2022a), while Atezolizumab (= Tecentriq), a PD-L1 inhibitor was approved by the FDA in 2016 (Eno, 2017), and by the European Commission in 2017 (EMA 2022b), both utilized in this project for production of caninized mAbs

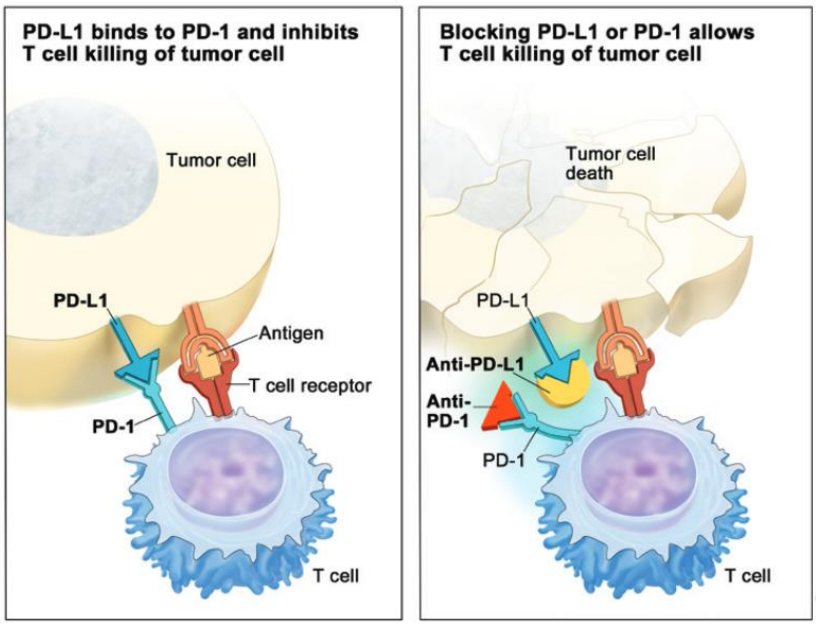

figure 3: Mechanism of immune checkpoint inhibitors (ICIs): Blockade of checkpoint molecule programmed cell death protein (PD-1)/programmed death-ligand 1 (PD-L1). (Left) Tumor cells overexpress PD-L1 on their surface and interact with PD-1 on immune effector cells such as T cells, which induces an inhibitory signal, blocking T cell proliferation, cytokine release and cytotoxic activity. (Right) Anti-PD-1 or anti-PD-L1 mAbs block the interaction between PD-1 and PD-L1, leading to restorage of T cell cytotoxic function and elimination of tumor cells (Eno, 2017).

1.5. Cancer in dogs

Cancer is the leading cause of death in dogs, resulting in approximately four million deaths per year (Gardner et al., 2016), however numbers are considered to be underestimated due to limited canine cancer registries. Existing cancer registries have different inclusion criteria, which is another issue (Boo et al., 2019). Cancer development in dogs occurs spontaneously (Gardner et al., 2016), with risk factors for tumor development ranging from age, breed and

thereby genetic predispositions, diet, living environment and other epidemiological factors (Wang et al., 2021). Research in comparative medicine has shown that similar cancer types found in humans and dogs were linked to shared environmental risk factors (Boo et al., 2019). The most common types of cancer in dogs include melanoma, osteosarcoma, lymphoma, lung cancer, mast cell tumor, mammary tumor and hemangiosarcoma. Cancers found in dogs share many similarities with human cancers, such as complex interactions between the immune system and developing tumors (Amin et al., 2020), heterogeneity of tumor cells and metastasis as common reason of death in dog cancer patients. Molecular pathways utilized by human tumors leading to evasion of immune surveillance are often observed upregulated in canine cancers as well, highlighting the similarities in tumorigenesis between species (Gardner et al., 2016).

1.6. Canine cancer treatments

For the treatment of canine cancers, surgery, radiotherapy, and chemotherapy are mostly used. However, surgery is only efficient for solid, non-metastasizing tumors, while chemotherapeutic agents destroy not only mutated tumor cells but also normal healthy cells with a high proliferation rate, causing additional harm (Jiang et al., 2019). In recent years, progress has been made in understanding the role of the immune system in cancer (Killick et al., 2015), a field of research referred to as immuno-oncology (Klingemann, 2018), and further in the research field of comparative oncology, investigating similarities in cancer between different species. This led to greater interest in the development of canine cancer immunotherapies, however progression is limited due to various factors including high costs and lack of knowledge about specific properties of the canine immune system and interactions within the TME (Klingemann, 2021).

Multiple clinical trials have been undertaken to investigate the effect of gene therapies in canine cancer patients, showing promising results leading to prolonged survival and an overall improve of life quality, however therapy success is often limited to a portion of responders (Glikin et al., 2014). Two DNA-based vaccines are currently approved by the USDA, one for the treatment of canine oral melanoma after surgical resection, encoding human tyrosinase, and one for the treatment of canine lymphoma. Nevertheless, studies undertaken were limited to comparison with historical controls, (Klingemann, 2021), further results were inconsistent in several clinical studies (Igase et al., 2020), and lack extended follow-up investigations (Zuleger et al., 2017). To date, there are no mAbs approved for the treatment of canine cancers. Two caninized mAbs received conditional approval by the USDA for treatment of lymphoma, anti-CD52 (Tactress®) and anti-CD20 (Blontress®), however no peer-reviewed data had been published, proving efficiency of these mAbs. Another pilot clinical study investigated the effects

of two therapeutic anti-PD-1 antibodies, one rat-dog chimeric and one caninized mAb, determining in vitro reactivity and blocking capacity of the PD-1/PD-L1 axis. Further, clinical efficacy was evaluated in a small number of dogs with advanced oral malignant melanoma and other tumors. The study showed promising results, confirming bioactivity as well as safety, however, follow-up trials as well as a larger number of canine cancer patients are required to prove beneficial effects. Surgical resection, radiation and/or chemotherapy were used in most canine cancer patients as first-line treatment (Igase et al., 2020). Another research group tested the effects of human ICIs in vitro in canine tissues, showing that anti-PD-L1 Atezolizumab increased T-cell cytokine production. The immunogenic potential of human proteins in dogs must be further investigated (Klingemann, 2021).

1.7. Canine PD-1 and PD-L1 in cancer

Consistent with data obtained from human cancers, PD-1 and PD-L1 expression levels are elevated in multiple malignant canine tumors (Klingemann, 2021), with PD-1 mainly expressed on tumor-infiltrating lymphocytes and PD-L1 expressed on tumor cells (Stevenson et al., 2021). Interaction between canine PD-1 and PD-L1 checkpoint molecules interferes with T cell activity, suppressing T cell proliferation and cytokine production (Igase et al., 2020), leading to immune evasion of tumor cells upon tumor progression (Maekawa et al., 2014). A study from 2016 investigated multiple canine cancer types, showing PD-L1 overexpression in oral melanoma, mast cell tumor, mammary carcinoma, prostatic cancer, osteosarcoma and histiocytic sarcoma, and PD-1 expressed at high levels on tumor-infiltrating lymphocytes, in samples obtained from oral melanoma. (Maekawa et al., 2016). PD-L1 overexpression was further found elevated in renal cell carcinoma, lymphoma, hemangiosarcoma and soft tissue sarcoma (Igase et al., 2020). In a study from 2021, the mRNA expression levels of PD-1, PD-L1 and PD-L2 were compared between canine patients with malignant melanomas or benign melanocytomas, showing that checkpoint molecule expression is significantly higher in malignant tumors. Furthermore, higher levels of checkpoint molecules were linked to an increased number of tumor-infiltrating lymphocytes in the TME, which is in line with findings obtained from human cancers (Stevenson et al., 2021). In another study of human lung adenocarcinoma and squamous cell carcinoma, an elevated level of PD-1 and PD-L1 in the TME correlated with a poor prognosis leading to shorter survival times and metastasis (Yeo et al., 2017), consistent with results from canine cancer studies (Stevenson et al., 2021).

1.8. Aim of the project

Despite the fact, that cancer is the leading cause of death in dogs, the development of canine anti-cancer immunotherapies lags far behind (Klingemann, 2018), (Klingemann, 2021). Current treatment for dog cancers includes surgery, chemotherapy, and radiotherapy (Adams

et al., 2010). Only few immunotherapies for dogs have been established so far, with therapy showing minor success, limited to some cancers. Further, pharmaceutical companies show minor interest in the research of potential canine tumor immunotherapies, as the market is limited and more profit is found in human cancer therapy (Klingemann, 2018). However, multiple studies highlight similarities between human and canine cancers, beginning at their clinical presentation, shared genetic characteristics (Schiffman et al., 2015) and molecular mechanisms up- or downregulated in the TME. Canine tumors were proven to evade immune surveillance by a row of mechanisms, that were also detected in human cancers (Amin et al., 2020). Checkpoint molecules PD-1, as well as PD-L1, were found upregulated in multiple canine cancers including malignant oral melanoma, mast cell tumor, mammary carcinoma, prostatic cancer, osteosarcoma, lymphoma, renal cell carcinoma, histiocytic sarcoma, hemangiosarcoma, and soft tissue sarcoma (Igase et al., 2020), highlighting the potential broad field of application among canine cancers. Human anti-PD-1 and anti-PD-L1 mAbs are used in clinics, showing promising results in prolonging life expectancy in multiple cancers (Jiang et al., 2019).

Therefore, the goal of this project was to generate caninized anti-PD-1 and anti-PD-L1 mAbs with specific canine IgG1 and IgG4 regions, aiming to provide a functional immunotherapy for the treatment of multiple canine cancers. Chimeric IgG mAbs were constructed to consist of variable heavy and light chains of human anti-PD-1 or anti-PD-L1 and constant heavy and light chains of canine IgG1 or IgG4 with approximately 50 kDa heavy chains and 25 kDa light chains *(figure 4).*

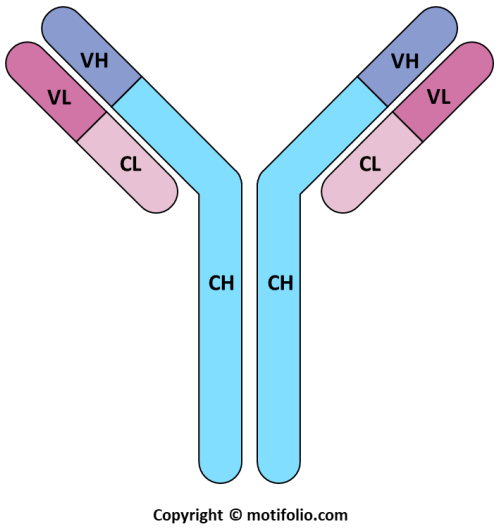

figure 4: Schematic representation of caninized mAbs consisting of canine constant IgG1 or IgG4 regions and human variable anti-PD-1 or anti-PD-L1. CH: constant heavy chain; CL: constant light chain; VH: variable heavy chain; VL: variable light chain (Adapted from motifolio.com)

1.9. Preliminary data from our lab

In preparation for the current project, aimed at producing caninized human/dog chimeric anti-PD-1 and anti-PD-L1 mAbs, pairwise sequence alignment analysis of human and canine PD-1 and PD-L1 protein sequences was conducted, followed by determination of binding capacities of human therapeutic anti-PD-1 and anti-PD-L1 mAbs on the canine macrophage-like cell like DH82, expressing both checkpoint molecules on its surface (Choi et al., 2020). These analyses aimed at predicting the potential efficacy of human anti-PD-1/PD-L1 mAbs to target canine checkpoint molecules. Further, plasmids encoding caninized mAbs were produced using a ligation independent cloning technique.

1.9.1. Analysis of human and canine PD-1/ PD-L1 protein sequences

Pairwise sequence alignment analysis of human and canine PD-1/ PD-L1 protein sequences was undertaken using the Software EMBOSS Needle webtool for the determination of identity between sequences. The results revealed that human and canine PD-1 protein sequences share 66.2 % identity, and 75.7 % identity between human PD-L1 and canine PD-L1 protein sequences *(figure 5 and 6).* The analysis demonstrates that human and canine PD-1 and PD-L1 share high concordance in their sequences.

figure 5: Pairwise sequence alignment of human and canine PD-1 protein sequences revealed 66.2 % identity.

figure 6: Pairwise sequence alignment of human and canine PD-L1 protein sequences resulted in 75.7 % consensus.

1.9.2. Binding affinities of human anti-PD-1/PD-L1 mAbs to canine PD-1/PD-L1 by flow cytometric analyses

The binding affinities of various therapeutic human anti-PD-1 and anti-PD-L1 mAbs to canine PD-1 and PD-L1 expressed by the macrophage-like cell line DH82 (Choi et al., 2020), were tested using fluorescent staining of human mAbs with fluorophore Allophycocyanin (APC) and flowcytometric analysis. The applied human mAbs targeting PD-1 were Pembrolizumab, Nivolumab and Cemiplimab, with Pembrolizumab showing the highest binding affinity to canine DH82 cells. The tested human mAbs targeting PD-L1 were Atezolizumab, Avelumab and Durvalumab, whereat Atezolizumab showed the highest binding capacity to canine DH82. Figure 7 visualizes the obtained results. Human therapeutic mAbs Pembrolizumab and Atezolizumab with the highest binding affinities to canine PD-1 and PD-L1 were chosen for production of caninized mAbs.

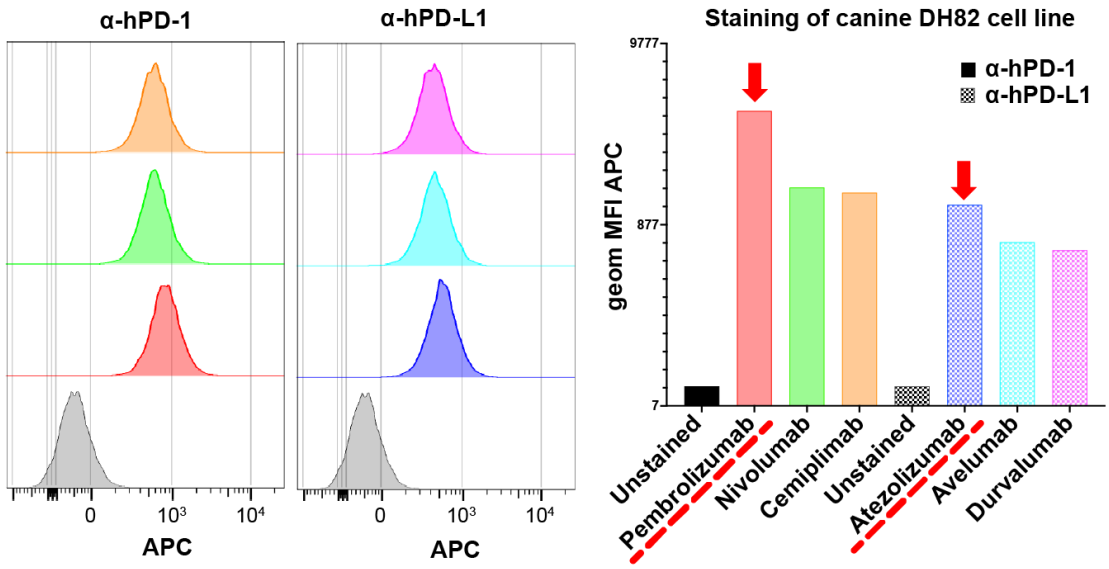

figure 7: Staining of canine macrophage-like cancer cell line DH82 with APC-labelled human therapeutic anti-PD-1 (Pembrolizumab, Nivolumab, Cemiplimab) and anti-PD-L1 antibodies (Atezolizumab, Avelumab, Durvalumab) revealed binding affinities via flow cytometric analyses. Pembrolizumab and Atezolizumab resulted in the highest binding capacities, as underlined in red.

1.9.3. Plasmid assembly

Plasmids encoding caninized mAbs were produced using Multiple overlap extension polymerase chain reaction (MOE-PCR), a ligation-independent cloning approach, thereby assembling four overlapping DNA fragments, as visualized in figure 8. Plasmids consist of a pVITRO1-hygro-msc backbone, variable heavy and light chain sequences encoding human anti-PD-1 or anti-PD-L1 and specific constant heavy and kappa light chain sequences of canine IgG1 or IgG4 as well as a hygromycin B resistance gene. Anti-PD-1 plasmids had a size of 8622 bp, while anti-PD-L1 isotypes were 8604 bp long. Competent *Escherichia coli*

(E. coli) cells were transformed with purified plasmids and positive clones were selected using hygromycin B.

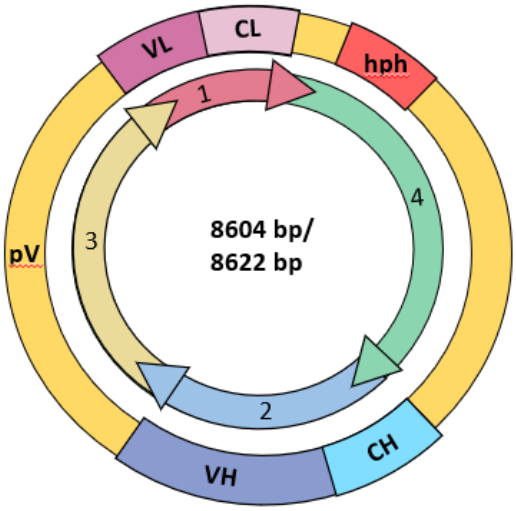

figure 8: Schematic depiction of circular plasmids of 8604 bp (anti-PD-L1) or 8622 bp (anti-PD-1) encoding caninized mAbs. Plasmids were assembled from four DNA fragments, as visualized in the inner circle. CH: constant heavy chain; CL: constant light chain; VH: variable heavy chain; VL: variable light chain; pV: pVITRO1-hygro-msc backbone; hph: hygromycin B resistance gene

1.10. Outlook of the applied methods

In the first phase of this Master thesis, growth conditions of recombinant *E. coli* cells were optimized, aimed at producing high yields of plasmid DNA for the following transfection. Plasmids were then purified and further sequenced. For production of mAbs, eukaryotic Expi293F cells were transfected, and antibodies were purified via affinity chromatography. SDS PAGEs, western blots and dot blots were performed for detection of mAbs. Binding capacities of APC-labelled human therapeutic mAbs Pembrolizumab (anti-PD-1) as well as Atezolizumab (anti-PD-L1) were further tested in the canine mammary carcinoma cell lines CF33, CF41 and canine osteosarcoma cell line D-17, evaluating PD-1/ PD-L1 expression and binding affinity in different canine cancer cell lines. Furthermore, binding affinities of human anti-PD-1 and anti-PD-L1 to in the human embryonic kidney cell line Expi293F used for transfection were determined. Thereby, we aimed to test the possible interference of checkpoint molecule expression on the production of mAbs by the Expi293F cell line. Our work aimed to establish an efficient, time-saving process to produce caninized mAbs at low cost for the potential treatment of canine cancers.

2. Materials

2.1. Primers

Table 1 provides an overview of the primers used for amplification of plasmid heavy and light chain DNA sequences. All primers were manufactured by the company Sigma-Aldrich and were used at concentrations of 10 µM.

table 1: Primers used for PCR amplification of heavy and light chains of plasmids and DNA sequencing.

Primer name	DNA sequence (5'-3')	Tm (°C)
Heavy chain_1 forward	24 bp; TTTGAGCG …… TCTCGGGC	54.2
Heavy chain_2 forward	20 bp; AACCCAAG …… TCCTCAGG	52.2
Light chain_1 forward	23 bp; CCGGAATG …… CACAACTC	52.2
pCEP_Reverse	20 bp; GTGGTTTG …… AACTCATC	49.7
RpVitro2	21 bp; CTCTAGAC …… AAGACCAG	59.5
Light chain_2 reverse	23 bp; ATCCCTAT …… CCACTCTC	55.3

2.2. Recombinant *E. coli* growth and plasmid DNA isolation

- Hygromycin B Selection Agar Plates:
  - 15 g Agar
  - 1 µl Hygromycin B (#1287.2, Carl Roth)
  - 5 g NaCl
  - 10 g Pepton
  - 5 g Yeast Extract
  - MiliQ H2O ad. 1 L
- Incubator: New Brunswick™ Innova ®42/42R Shaker (Eppendorf)
- Plasmid Miniprep System: PureYield™ Plasmid Miniprep System (#A1222, Promega)
- Plasmid Midiprep System: GenElute™ Plasmid Midiprep Kit (#PLD-35, Sigma-Aldrich)
- sterile 0.2 µm PES filters: Nalgene® syringe filter units, disposable, polyethersulfone (PES) membrane (#Z741696, Merck)
- Spectrophotometer: NanoPhotometer Pearl (Implen)
- LB medium
  - 1 µl Hygromycin B
  - 5 g NaCl
  - 10 g Pepton

  - 5 g Yeast Extract
  - MiliQ H2O ad. 1 l
- LB+ medium
  - 3.96 g 1M Glucose
  - 0.5 g 1M MgSO4
  - 0.015 g 1 M CaCl
  - LB medium ad. 1 l
- TB medium
  - 5 g Glycerol
  - 24 g Yeast Extract
  - 12 g Tryptone
  - MiliQ H2O ad. 0.9 L
  - 2.31 g 0.17 M Potassium dihydrogen phosphate (KH2PO4)
  - 12.54 g 0.72 M Dipotassium hydrogen phosphate (K2HPO4)
  - MiliQ H2O ad. 100 ml

2.3. PCR, enzymatic digestion and DNA sequencing

- PCR Thermocycler: TProfessional BASIC 96 Gradient (Biometra)
- Green Tag buffer: GoTaq® Buffer (#M791A, Promega)
- dNTPs: dNTP Set (100 mM) (#10297-018, Thermo Fisher Scientific)
- GoTaq Polymerase: GoTaq® G2 DNA Polymerase (#M784B, Promega)
- Midory Green: Midory Green Advance DNA Stain (#MG04, Nippon Genetic Europe GmbH)
- Gel loading dye: Gel Loading Dye, Purple (6X) (#B7024S, New England Biolabs)
- DNA ladder: Quick-Load® Purple 1 kb Plus DNA Ladder (#N0550, New England Biolabs)
- Imager: ChemiDoc™ touch imaging system (Bio-Rad Laboratories)
- Restriction enzymes:
- BstXI (#ER1021, Thermo Fisher Scientific)
- EcoRI-HF (#R3101S, New England Biolabs)
- 10 X rCutSmart Buffer: rCutSmart™ Buffer (#B6004S, New England Biolabs)
- 10 X NEBuffer r3.1: NEBuffer™ r3.1 (#B6003S, New England Biolabs)
- Heater: BioShake iQ (QInstruments)
- DNA Sequencing kit: Mix2Seq Kit NightXpress (Eurofins Genomics)
- Image Lab™ Software (Bio-Rad Laboratories)
- UGENE Software (Unipro) (Okonechnikov et al., 2012)

2.4. Human Expi293F cell line

- Expi293F™ cells (#A14527, Thermo Fisher Scientific)
- Expi293F™ Expression medium (#A1435102, Thermo Fisher Scientific)
- SFM4HEK293 medium: HyClone SFM4HEK293™ media (#SH30521.02, Cytiva)
- High glucose DMEM medium: Dulbecco's Modified Eagle's Medium - high glucose (#D5671, Sigma-Aldrich), supplemented with: 10 % Fetal bovine serum (FBS), 2 mM L-glutamine
- Counter: CellDrop™ (DeNovix)
- Incubator: BBD 6220 CO2 Incubator, 220 L, Polished Stainless Steel (Thermo Fisher Scientific)
- Cell culture flasks:
- Corning® Erlenmeyer cell culture flasks:
  - 125 ml (#CLS431143, Merck)
  - 250 ml (#CLS431144, Merck)
- Falcon® Rectangular Canted Neck Cell Culture Flask with Vented Cap:
  - 25 cm^2 (#353109, Corning)
  - 75 cm^2 (#353136, Corning)
- 24-well plate: Falcon® 24-well Clear Flat Bottom TC-treated Multiwell Cell Culture Plate (#353047, Corning)

2.5. Canine cancer cell lines

- CF33: CF33.Mg, *Canis familiaris,* Mammary carcinoma (#CRL-6227, ATCC Discontinued)
- CF41: CF41.Mg, *Canis familiaris,* Mammary carcinoma (#CRL-6232, ATCC)
- D-17: D-17, *Canis familiaris*, Osteosarcoma (#CCL-183, ATCC)
- DH82: DH82, *Canis familiaris*, Macrophage-like cell, Malignant Histiocytosis (#CRL-10389, ATCC)
- High glucose DMEM medium: (see Materials 2.4.), supplemented with: 10 % Fetal bovine serum (FBS), 1 % Penicillin/Streptomycin (Pen Strep), 2 mM L-glutamine
- Incubator: see Materials 2.4.

2.6. Transfection and antibody harvest

2.6.1. Transfection of eukaryotic Expi293F cells in suspension

- ExpiFectamine™ 293 Transfection Kit (#A14525, Thermo Fisher Scientific)

- Opti-MEM I Medium: Opti-MEM I Reduced Serum Medium (#11058021, Thermo Fisher Scientific)
- Hygromycin B (see Materials 2.2.)

2.6.2. Transfection of adherent eukaryotic Expi293F cells

- Lipofectamine LTX transfection kit: Lipofectamine™ LTX Reagent with PLUS™ Reagent (#15338030, Thermo Fisher Scientific)
- Opti-MEM I Medium (see Materials 2.6.1.)
- Hygromycin B (see Materials 2.2.)
- Incubator (see Materials 2.4.)

2.7. Antibody harvest and purification via affinity chromatography

- PES filter system: Stericup Quick Release-GP Sterile Vacuum Filtration System (#S2GPU05RE, Merck)
- Protein A affinity column: HiTrap® Protein A High Performance (#GE29-0485-76, Merck)
- Chromatography system: NGC Quest 10 Chromatography System (Bio-Rad Laboratories)
- Dialysis system: Tube-O-DIALYZER™, Medi, 15K MWCO (#786-618, G-Biosciences)

2.8. Antibody control assays

2.8.1. SDS-PAGE and Silver staining

- 15 % resolving gel (for 8 gels):
  - 24 ml 30 % acrylamide (#A36260500, AppliChem, Darmstadt, Germany)
  - 12 ml lower buffer (0.4 % SDS, 1.5 M tris, ultrapure water, pH 8.8)
  - 12 ml ultrapure water
  - 24 µl TEMED (#T7024-50ML, Sigma-Aldrich, MO, USA)
  - 240 µl 10 % APS (#A3678, Sigma-Aldrich, MO, USA)
- 4.5 % stacking gel (for 8 gels):
  - 2.4 ml 30 % acrylamide
  - 4 ml upper buffer (0.4 % SDS, 0.5 M tris, ultrapure water, pH 6.5)
  - 9.6 ml ultrapure water
  - 8 µl TEMED
  - 160 µl 10% APS
- Reducing sample buffer (4 x): 200 mM tris, 300 mM DTT, 8 % SDS, 40 % glycerol, 40 mg bromophenol blue in 50 ml ultrapure water

- Non-reducing sample buffer (4 x): see reducing sample buffer, without DTT
- Protein ladder:
  - PageRuler™ Prestained Protein Ladder, 10 to 180 kDa (#26616, Thermo Fisher Scientific)
  - Spectra™ Multicolor High Range Protein Ladder (#26625, Thermo Fisher Scientific)
  - PageRuler™ Plus Prestained Protein Ladder, 10 to 250 kDa (#26619, Thermo Fisher Scientific)
- Electrophoresis buffer (10 x): 250 mM tris, 1.92 M glycine, 1 % SDS, pH 8.3
- Heater: BioShake iQ (QInstruments)
- SDS-PAGE device: Mini-PROTEAN®tetra system (Bio-Rad Laboratories)
- Gel fixing solution: 50 ml EtOH, 10 ml Acetic Acid, 40 ml ultrapure water
- Wash solution: 30 ml EtOH, 70 ml ultrapure water
- Thiosulfate reagent: 100 mg (0.02 %) sodium thiosulfate (Na2S2O3), 500 ml ultrapure water
- Silver nitrate reagent: 1 g (0.2 %) Silver nitrate, 100 µl (0.02 %) Formaldehyde (37 %), 50 ml ultrapure water (stored at RT protected from light)
- Developer solution: 15 g Sodium Carbonate (Na2CO3), 250 µl (0.05 %) Formaldehyde (37 %), 2.5 mg Sodium thiosulfate 500 ml ultrapure water (stored at 4 °C)
- Stop solution: 2.5 g Glycine (0.5 %) 500 ml ultrapure water (stored at 4 °C)
- Imager: see Materials 2.3.

2.8.2. Dot blot

- Nitrocellulose membrane: Amersham™ Protran™ 0.2 µm NC (#10600001, GE Healthcare)
- Canine total IgG (positive control): Dog purified IgG (10 mg/ml) (#AS122624, Agrisera)
- Anti-dog IgG antibody: Peroxidase AffiniPure Rabbit Anti-Dog IgG, Fc fragment specific (#304-035-008, Jackson Immuno Research), HRP conjugated
- TBS-T (tris-buffered saline with tween): 0.05 M tris, 0.15 M NaCl, 0.05 % Tween-20, pH 7.4
- Substrate solution: Clarity Western ECL Substrate (#1705061, Bio-Rad Laboratories)
- Imager: see Materials 2.3.

2.8.3. Western blot

- Materials used for SDS-PAGE: see Materials 2.8.1.

- Canine total IgG, anti-dog IgG antibody, TBS-T and substrate solution: see Materials 2.8.2.
- Trans-Blot® Turbo™ Transfer Pack (#17041158, Bio-Rad Laboratories)
- Transfer cassette and device: Trans-Blot® Turbo™ transfer system (#1704150, Bio-Rad Laboratories)
- Imager: see Materials 2.3.

2.9. Flow cytometric analysis

- Alexa Fluor Antibody Labeling Kit: Alexa Fluor® 647 Antibody Labeling Kit 650/668 (#A20186, Thermo Fisher Scientific)
- Human Pembrolizumab (Keytruda), human Atezolizumab (Tecentriq): kindly donated by The Hospital Pharmacy (APO), Central Cytostatics, Preparation of the Vienna General Hospital (AKH)
- Human IgG mAb: Immunoglobulin G (IgG), Normal Human Plasma (10 mg/ml) (#16-16-090707, Athens research and technology)
- Canine total IgG: see Materials 2.8.2.
- Staining buffer: Cell staining buffer (#420201, BioLegend)
- Zombie Violet solution: Zombie Violet™ Fixable Viability Kit (#423114, BioLegend)
- FACS tubes: microtube 1.2 ml bulk PP (#I1412-0000, Starlab)
- Flow cytometer: FACS Canto II (BD Biosciences)
- FlowJo™ version 10 (FlowJo, LLC)

3. Methods

3.1. Recombinant *E. coli* growth and plasmid DNA isolation

Plasmid DNA isolation from recombinant *E. coli* cells was performed using a Plasmid Miniprep system for determination of plasmid yields in different growth media, while a Plasmid Midiprep system was used subsequently in the context of producing higher yields of plasmid DNA, required for transfection of eukaryotic cells.

3.1.1. Optimization of *E. coli* growth and DNA plasmid yield

3.1.1.1. Growth conditions and OD_{600} measurement

Recombinant *E. coli* cells were cultured in three different growth media, aimed at determining optimal growth conditions for high yields of each plasmid isotype. The used growth media were low salt Lysogeny Broth (LB) media, supplemented low salt LB (LB+) media and Terrific Broth (TB) media. Transformed *E. coli* cells stored within glycerol stocks were scratched from the

frozen stocks using a pipet tip, spread on hygromycin selection agar plates (75 µg/ml hygromycin B) and grown overnight at 37 °C. The next day, starter cultures were produced. Therefore, a single *E. coli* colony of each plasmid isotype was picked from the agar plate using a pipette tip and resuspended in 100 µl LB medium with hygromycin B (50 µg/ml). Further, 25 µl cell suspension were transferred to 3 ml of each culture medium containing hygromycin B (50 µg/ml) and let grow for 8 hours at 37 °C, 250 rpm. Starter cultures were then used at a ratio of 1: 50 000 to inoculate main cultures (5 ml) for 17 hours at 37 °C and 250 rpm. The following day, optical densities at a wavelength of 600 nm (OD_{600}) were measured using a spectrophotometer.

3.1.1.2. Plasmid DNA isolation and concentration determination

Following overnight growth of recombinant *E. coli* colonies in 3 different culture media, plasmid DNA was isolated using a Plasmid Miniprep system. First, 1.2 ml of each bacterial culture were transferred to 1.5 ml tubes and centrifuged (20 000 x g, 30 sec, RT) in a microcentrifuge. The supernatant was discarded and an additional amount of 1.2 ml bacterial culture was added to the same tube, repeating the centrifugation step. Next, the supernatant was removed and 600 µl of ultrapure water were subjoined to the cell pellet, resuspending the cells completely by pipetting up and down. An amount of 100 µl Cell Lysis Buffer was added to each tube, resuspending the mixture again. Next, 350 µl of cold (4–8 °C) Neutralization Solution was added, inverting the tubes for resuspension. The tubes were centrifuged (20 000 x g, 3 min, RT). The supernatant of each tube was transferred to a PureYield™ Minicolumn without disturbing the cell debris pellet. The minicolumns were placed in 1.5 ml collection tubes and centrifuged (20 000 x g, 15 sec, RT). The flowthrough was discarded and the minicolumns were placed into the same collection tubes. Next, 200 µl of Endotoxin Removal Wash were added to the columns and the tubes were centrifuged (20 000 x g, 15 sec, RT). Then, 400 µl of Column Wash Solution were added to each tube and centrifuged (20 000 x g, 30 sec, RT). Each column was transferred to a 1.5 ml microcentrifuge tube and 30 µl of Elution Buffer were directly added to the minicolumn matrix. The tubes were incubated at RT for one minute and then centrifuged (20 000 x g, 15 sec, RT) to elute the plasmid DNA. Minicolumns were discarded and the eluted plasmid DNAs were stored at -20 °C. DNA concentrations were determined using a spectrophotometer at a wavelength of 260 nm.

3.1.2. Plasmid production

Starter cultures were prepared in 3 ml of the chosen growth medium, as described in Methods 3.1.1.2., adding hygromycin B to a concentration of 50 µg/ml. Next, overnight cultures were prepared, using 40 ml of culture media with hygromycin B (50 µg/ml). Starter cultures were added at a ratio of 1: 50 000. *E. coli* cells were incubated at 37 °C and 250 rpm for 17 h.

The next day, the OD_{600} of each bacterial culture was measured using a spectrophotometer. The obtained values were used to calculate the volume of each bacterial culture required for the isolation of DNA via a Plasmid Midiprep system. A total cell mass of 80 is suggested to be used, whereas cell mass equals OD_{600} x ml of culture. For low copy plasmids, a total cell mass of 160 is suggested. The calculated amount of each cell culture was transferred to a 50 ml tube and centrifuged (4 000 x g, 10 min, RT). The supernatant was discarded, and the pellet was completely resuspended in 1.2 ml of Resuspension Solution by pipetting up and down until homogenous. Next, cells were lysed, adding 1.2 ml of Lysis Solution. Tubes were gently inverted several times for resuspension, until the mixture was clear and viscous. Cell lysis might not exceed five minutes. An amount of 1.6 ml Neutralization Solution was added to each tube, mixing again by gentle inversion. The mixtures were transferred to 1.5 ml microcentrifuge tubes and centrifuged (15 000 x g, 15 min, RT). In the meantime, the DNA binding columns were inserted into 15 ml collection tubes and 3 ml of Column Preparation Solution was added to each column. The tubes were centrifuged (4 000 x g, 2 min, RT) and the flowthrough was discarded. The cleared lysate was transferred to the columns and the tubes were again centrifuged (4 000 x g, 2 min, RT). Next, 3 ml Wash Solution was added to the column, repeating centrifugation (4 000 x g, 5 min, RT). In the meantime, 1 ml of Elution Solution for each sample was heated to 65 °C. The columns were then transferred to fresh 15 ml tubes, adding 1 ml of preheated Elution Solution to each column. The columns were incubated for 10 minutes at RT before centrifuging (4 000 x g, 5 min, RT). The obtained DNA concentrations were measured by use of a spectrophotometer at a wavelength of 260 nm. For use in the transfection of eukaryotic cells, DNA samples were filtrated through sterile 0.2 µm PES filters.

3.2. Plasmid DNA control assays

3.2.1. PCR and enzymatic digestion

Following purification of DNA plasmids from recombinant *E. coli* cells, PCR reactions were performed amplifying the heavy as well as the light chains of the 4 plasmids, serving as control. The applied primers for amplification of the heavy chain sequence of all plasmids were “Heavy chain 1 forward” and “pCEP Reverse”, whereas two primer pairs served for amplification of the light chain sequences: “Light chain 1 forward” together with “Light chain 2 reverse” as well as “Light chain 1 forward” in combination with “RpVitro 2”. For each PCR reaction, 10 µl Green tag buffer were mixed with 1 µl dNTPs, 0.4 µl forward and reverse primer, 0.2 µl GoTaq Polymerase and 220 ng plasmid DNA, adding ultrapure water to a final volume of 50 µl. PCR conditions applied for amplification of heavy and light chain sequences of the purified DNA plasmids are outlined in table 2. Following PCR, amplified DNA fragments were separated electrophoretic on agarose gels. Agarose gels were produced at concentrations

between 0.6 – 1 %, depending on the size in bp of DNA to be separated. To produce a 1 % agarose gel, 4 g agarose was dissolved in 400 ml 1 x TAE buffer and microwaved, swirling the flask occasionally, until the agarose was completely dissolved. After letting the agarose solution cool down to a temperature of 55- 60 °C, 15 µl of Midory Green was added and the solution was poured into the prepared gel tray, letting set until solidified. Meanwhile, samples were mixed with Gel loading dye and then samples as well as a DNA ladder were loaded to the gel. The gel was run in 1 x TAE buffer at 90 V, 90- 120 minutes. For visualization of the separated DNA fragments, the imager was used. The software “Image Lab” was used to determine the concentration of DNA present in each PCR sample.

table 2: PCR amplification of the heavy and light chain DNA sequences of the purified DNA plasmids.

Step	T (°C)	Time (s)	Repeats
Initial denaturation	95	5 min	/
Denaturation	95	30	30
Annealing	53	30	
Extension	72	30	
Final Extension	72	10 min	/
Hold	4	∞	/

Enzymatic digestion of PCR- amplified heavy and light chain DNA sequences was performed with two restriction enzymes. EcoRI-HF targets restriction sites in the DNA region encoding the antibody heavy chain, while the restriction enzyme BstXI digests plasmids within the light chain DNA region. For each enzymatic digestion reaction 1 µg of plasmid DNA was used. Samples were prepared as summarized in tables 3 and 4 and enzymatic digestion was performed heating samples at 37 °C, for 12 minutes, followed by heat inactivation for 20 minutes at 65 °C for EcoRI-HF and at 80 °C for BstXI. Digested samples were separated on agarose gels by electrophoresis.

table 3: Enzymatic digestion of heavy chain DNA sequences using the restriction enzyme EcoRI-HF.

Component	Amount
EcoRI-HF	1 µl
DNA (heavy chain)	1 µg
10 X rCutSmart Buffer	5 µl
H_2O (Milli-Q)	Ad. 50 µl

table 4: Enzymatic digestion of light chain DNA sequences via the restriction enzyme BstXI.

Component	Amount
BstXI	1 µl
DNA (light chain)	1 µg
10 X NEBuffer r3.1	5 µl
H2O (Milli-Q)	Ad. 50 µl

3.2.2. Plasmid DNA sequencing and alignment via UGENE

Purified plasmid DNAs were sequenced using the Mix2Seq overnight kit provided by the company Eurofins, which recommends a DNA concentration of 50-100 ng/µl. An amount of 15 µl of plasmid DNA was mixed with 2 µl primer. For amplification of heavy chain sequences of all plasmids the primers “Heavy chain_1 forward” or “pCEP_Reverse” were used, while “Light chain_1 forward” or “RpVitro2” were applied for amplification of light chain regions. The primer “Heavy chain_2 forward” was additionally applied for amplification of heavy chain sequence of pVITRO-Atezo-IgG4. For alignment and comparison of the obtained DNA sequences with the sequences of the in silico constructed plasmids, the software UGENE was used.

3.3. Expi293F cell maintenance and viability

Eukaryotic Expi293F™ cells were cultured in 125 ml baffled Erlenmeyer flasks in 25 ml Expi293TM Expression Medium. Cells were maintained in an incubator at 37 °C with 8 % CO2 and ≥80% relative humidity on an orbital shaker at 125 rpm. Expi293F cells were passaged at a density of approximately 3 – 5 × 10^6 viable cells/ml, typically twice a week, diluting them to a concentration of 0.3 x 10^6 – 0.5 x 10^6 cells/ml. Expi293F cells were further cultured in SFM4HEK293 medium in parallel, comparing cell viability in both media under equal conditions. Therefore, fresh batches of Expi293F cells containing 107 cells were thawed and transferred to 50 ml of each culture media in 250 ml flasks. Cells were maintained under equal conditions. Over a period of four weeks, cells were passaged twice per week, monitoring cell viability using an automated cell counter and trypan blue.

3.4. Canine cancer cell maintenance

Canine carcinoma cell lines CF33, CF41 and canine osteosarcoma cell line D-17 were cultured in high-glucose DMEM medium supplemented with 10 % Fetal bovine serum (FBS), 1 % Penicillin/Streptomycin (Pen Strep) and 2 mM L-glutamine. They were maintained in an incubator at 37 °C.

3.5. Transfection and antibody harvest

3.5.1. Transfection of eukaryotic Expi293F cells in suspension

The Expi293F cells were cultured in suspension with Expi293™ Expression Medium under shaking conditions, as summarized in Methods 3.3. One day prior to transfection, Expi293F™ cells were expanded to a cell density of approximately 2.5 – 3 × 10^6 viable cells/ml in 25 ml of medium per transfection. Cell cultures were incubated on the shaking platform for 20 hours. The next day, cell density and viability were determined using an automated cell counter and

trypan blue at a ratio of 1:1. Density should be 4.5 – 5.5 x 10^6 cells/ml and viability must be ≥95 %. For each transfection, a volume of cell culture containing 7.5 x 10^7 cells was transferred to a 50 ml conical tube and centrifuged (300 x g, 5 min, RT). Following centrifugation, the supernatant was discarded, and the cells were carefully resuspended in 25.5 ml of fresh medium. The cell suspension was transferred to a fresh 125 ml baffled Erlenmeyer flask and placed back on the shaker in the incubator until used. In the next step, 30 µg of plasmid DNA were diluted with Opti-MEM I Medium to a final volume of 1.5 ml and mixed gently by inversion. Then, 81 µl of ExpiFectamine™ 293 Reagent were diluted with Opti-MEM I Medium up to a volume of 1.5 ml, mixed gently by inverting and incubated at RT for 5 min. The solutions were put together and mixed gently by inversion, then incubated at RT for 20 minutes for the formation of lipid-DNA complexes. In the next step, the complex solution was slowly transferred to the cells, swirling the culture flask gently during addition. Cells were placed on the shaking platform again and incubated for 20 hours. The next day, 150 µl of Expifectamine™ 293 Transfection Enhancer 1 were mixed with 1.5 ml of Expifectamine™ 293 Transfection Enhancer 2 and added to each flask. The following day, hygromycin B was added to each flask to a final concentration of 50 µg/ml. Seven days after transfection, antibodies were harvested.

3.5.2. Transfection of adherent eukaryotic Expi293F cells

The Expi293F cell line was cultured in suspension with Expi293™ Expression Medium under shaking conditions, as described in Methods 3.3. For all following steps in adherent transfection, complete Dulbecco's Modified Eagle's Medium (DMEM) high glucose, supplemented with 10 % fetal bovine serum (FBS) and 1 % L-glutamine, was used. One day before transfection, cells were transferred to 24-well plates, seeding 2 x 10^5 cells per well in 500 µl of DMEM medium. Cells were let grown overnight in an incubator with 8 % CO_2 at 37 °C. The next day, cells were transfected, presuming 90 % of confluence. The Lipofectamine LTX transfection kit was used, including the PLUS™ reagent for enhanced transfection efficiency. First, the growth medium was removed and replaced with 500 µl of fresh medium. For each well of cells to be transfected, 810 ng of plasmid DNA were diluted to a final volume of 50 µl with Opti-MEM I Medium, adding 1 µl PLUS™ reagent. Per transfection, 2.5 µl Lipofectamine LTX reagent was mixed with Opti-MEM I Medium up to a volume of 50 µl. The solutions were then put together, mixed gently by inversion, and incubated for 30 minutes at RT for the formation of DNA- Lipofectamine LTX complexes. After incubation, 100 µl of complex solution were slowly added to each well and the plates were mixed gently by rocking the plate back and forth. A mock transfection without plasmid was performed in parallel, serving as a negative control. Cells were again incubated overnight. After 16 hours, cells were detached, removing the medium and adding 200 µl Accutase solution. The reaction was stopped by the addition of 500 µl DMEM complete medium. Cells were centrifuged (150 x g, 5 min, RT) and the

supernatant was replaced with DMEM medium, diluting cells 1:10 and distributing among 10 wells. The following day, the growth medium was replaced by DMEM complete medium supplemented with 200 µg/ml hygromycin B. After 3 days, the selective medium was replaced, adding different concentrations of hygromycin B to the wells (50 µg/ml, 100 µg/ml, and 200 µg/ml). The selective medium was then replaced every 3 days, until the cells from the mock transfection were all dead. In the following, positive clones were expanded further to bigger flasks of 25 cm^2 and further 75 cm^2, changing the growth medium every 3 days. Three weeks after transfection, confluent cells were detached using Accutase solution and adapted for growth in suspension in Expi293™ Expression Medium under shaking conditions. A set of mAb-producing cells were further detached using Accutase solution and frozen at -80 °C in FBS adding 10 % DMSO. Expi293F cells were thawed after 2 weeks and cultured in DMEM complete medium under adherent conditions. Four days after thawing, hygromycin B was added at a concentration of 100 µg/ml. After 7 days of cell growth in suspension, mAbs in the supernatant were harvested.

3.5.3. Antibody harvest

For mAb harvest, the cell suspension of each flask was transferred to a 50 ml conical tube and centrifuged (280 x g, 7 min, RT). The centrifugation step was repeated, adding the cell supernatant to a fresh tube. Next, the supernatant was transferred to a high-speed centrifuge tube, centrifuged (20 000 x g for 30 min, 4 °C) and diluted 1:1 with 1 M phosphate-buffered saline (PBS). The dilution was filtrated using a 0.22 µm PES filter and stored at 4 °C until purification. A protease inhibitor cocktail and 0.1 M sodium azide were added to the filtrated supernatant at a ratio of 1:100 to ensure the stability of mAbs, which was stored at 4 °C.

3.6. Antibody purification via affinity chromatography

MAbs were purified using Protein A affinity columns with column volumes of 0.96 ml and a chromatography system. The applied program is summarized in table 5. The column was equilibrated with 1 M PBS (pH 7.4) and 0.1 M citric acid (pH 2.7) was used for elution of mAbs. All buffers and the sample were degassed before usage. Following affinity chromatography, antibody concentrations were determined using a spectrophotometer. Samples were dialyzed against PBS at 4 °C overnight on a magnetic stirrer and PBS was exchanged twice. The solution was transferred to a new tube and stored at 4 °C. Protease inhibitor cocktail and 0.1 M sodium azide were added to the dialyzed samples at a ratio of 1:100 and stored at 4 °C.

table 5: Overview of the applied chromatography program containing its consecutive steps, buffers, flow rates, the volume of each buffer applied in column volumes (CV) and fraction volumes collected per step. The sample volume (supernatant) varied between 25- 50 ml. CV= 0.96 ml

Step	Flow rate (ml/min)	Buffer	V (CV)	V (fraction) (ml)
Equilibration	1	1 M PBS	10	/
Sample application	0.2	Supernatant	n/a	12
Column wash I	1	1 M PBS	14	12
Elution I	1	gradient flow PBS, citric acid	19	1
Elution II	1	0.1 M Citric acid	5	1
Column wash II	1	1 M PBS	10	5
Column wash III	1	20 % Ethanol	20	/

3.7. Antibody control assays

3.7.1. SDS-PAGE and Silver staining

For sodium dodecyl sulphate polyacrylamide gel electrophoresis (SDS-PAGE), a 15 % acrylamide resolving gel was prepared and on top a 4.5 % acrylamide stacking gel was casted, each allowing to polymerize for one hour. Samples were mixed with reducing as well as non-reducing sample buffer (4X) and denatured at 95 °C for 5 min. Next, samples as well as protein ladder were loaded and the gel was run in electrophoresis buffer at 110 V for approximately 90 minutes until the sample buffer reached the bottom of the gel. All steps of silver staining were performed at RT under gentle agitation. After the electrophoretic run, the gel was washed briefly with distilled water and then incubated in Gel fixing solution for 60 minutes under gentle agitation. Following three washing steps using the Wash solution for 20 minutes each time, the gel was incubated one minute in Thiosulfate reagent. Next, SDS-PAGE was washed 3 times for 20 seconds with ultrapure water. The gel was incubated for 20 minutes in the Silver nitrate reagent and subsequently rinsed twice with ultrapure water. Developer solution was added for 2- 15 minutes until desired band sensitivity was reached, adding Stop solution as last step for 5 minutes. The gel imager was used for visualization of protein bands on the gel.

3.7.2. Dot blot

On a nitrocellulose membrane, 2 µL of each sample as well as canine total IgG, which was used as positive control, were spotted twice, allowing the membrane to dry for one hour at RT.

All following steps were performed at RT. After blocking unspecific binding sites with 5 % milk in 1 x TBS-T for one hour under gentle agitation, the membrane was rinsed with 1 x TBS-T and incubated in 1 x TBS-T on a shaking platform for 15 minutes. Anti-dog IgG antibody was diluted 1: 3000 in 1 x TBS-T, adding milk powder to a concentration of 5 %, incubating the membrane for two hours under gentle agitation. Following two washing steps in 1 x TBS-T for 10 minutes, membranes were incubated in 2 ml of substrate solution for 5 min in the dark and then analysed using the gel imager.

3.7.3. Western blot

Samples as well as canine total IgG, serving as positive control, were mixed with reducing as well as non-reducing sample buffer and run on an SDS-PAGE. Following SDS-PAGE (as summarized in Methods 3.8.1.), the gel was blotted onto a nitrocellulose membrane. Therefore, components were assembled in a transfer cassette as follows: bottom cassette; 2 filter papers soaked in transfer buffer; nitrocellulose membrane; gel; 2 filter papers soaked in transfer buffer; top cassette. The transfer chamber was placed into the transfer device and the program “Turbo – 1 Mini Gel TGX – Mixed MW (2.5 A, 25 V, 3 min)” was applied. Following transfer, membranes were rinsed with 1 x TBS-T and then incubated with 5 % milk in 1 x TBS-T for 1 h at RT under gentle agitation to block unspecific binding sites. Membranes were washed twice for 10 minutes with 1 x TBS-T and then incubated with anti-dog IgG antibody diluted 1:3000 in 1 x TBS-T with 5 % milk for 2 hours, at RT under gentle agitation. After washing three times with 1 x TBS-T for 10 min, 2 ml substrate solution was added to the membrane and incubated for 5 min at RT in the dark before analysis on the imager.

3.8. Flow cytometric analysis: Determination of binding capacity

For flow cytometric analysis, human anti-PD-1 and anti-PD-L1 mAbs were labeled with the fluorophore Allophycocyanin (APC) using the Alexa Fluor Antibody Labeling Kit. Therefore, antibodies were diluted in Hanks’ Balanced Salt Solution (HBSS), to a concentration of 1 mg/ml, adding 1 M sodium bicarbonate at a ratio of 1:10. An amount of 100 µl of diluted mAbs was transferred to the vial of Alexa Fluor dye, mixed by inversion, and incubated at RT for 1 hour. Next, the purification column was assembled adding 1.5 ml of the resin bed and centrifuged (1100 x g, 3 min, RT). The reaction mix was then transferred to the column and centrifuged (1100 x g, 5 min, RT), to collect the labeled antibodies. For determination of binding capacity, counted cells were centrifuged (300 x g, 5 min, RT), the supernatant was removed, and 10^5 cells were resuspended in 50 µl Zombie Violet solution, diluted 1:800 in HBSS, for live/dead discrimination. APC-labelled antibodies were added to a final concentration of 40 µg/ml, and 200 µg/ml canine/ human IgG, depending on the origin of cell line, was used to block unspecific binding sites. Cells were incubated for 30 minutes at 4 °C,

protected from the light. Stained cells were washed twice using 300 µl Cell staining buffer and centrifuged after each wash step (300 x g, 5 min, RT). The supernatant was removed, and cells were resuspended in 100 µl Cell staining buffer. Simultaneously, two tubes were prepared as negative controls, one tube containing cells diluted in Cell staining buffer and one tube with cells in staining buffer and human or canine IgG. Samples were acquired via flow cytometry. Gating strategy for determination of binding capacity of APC-labelled mAbs to canine and human cells is shown in figure 9. Data analysis was carried out using the software FlowJo™ version 10.

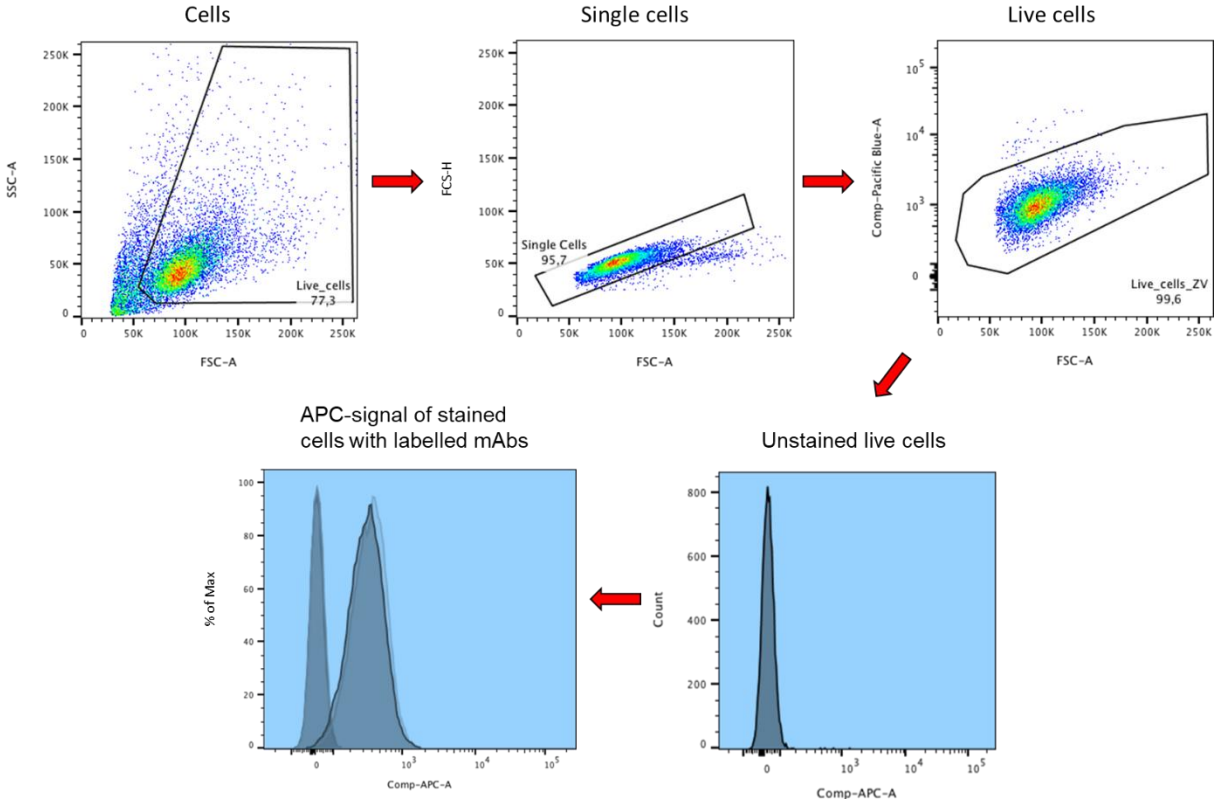

figure 9: Gating strategy for determination of binding capacity of APC-labelled human anti-PD-1 and anti-PD-L1 mAbs to human Expi293F cells and canine cancer cell lines CF33, CF41 and D-17.

4. Results and Discussion

4.1. Recombinant *E. coli* growth and plasmid DNA isolation

An initial objective of the project was to identify optimal growth conditions for recombinant *E. coli* cells of each plasmid isotype. Growth conditions were evaluated by measuring the OD_{600} and plasmid concentrations after growth in three different culture media. In the next step, optimized conditions were applied to produce plasmids at high concentrations and purity.

4.1.1. Optimization of *E. coli* growth and DNA plasmid yield

4.1.1.1. Growth conditions and OD600 measurement

This analysis was undertaken to identify the optimal culture medium for recombinant *E. coli* cells with different plasmid isotypes. Three different growth media were tested, including LB medium, supplemented LB medium (LB+), and TB medium. The first set of analyses examined the impact of growth medium on recombinant *E. coli* biomass production, evaluated via measurement of optical density at a wavelength of 600 nm (OD_{600}), as visualized in figure 10. LB medium is a nutrient-rich medium commonly used for cultivation of members of the *Enterobacteriaceae,* promoting fast bacterial growth and resulting in good plasmid yields (Macwilliams et al., 2016). LB+ medium was supplemented with a combination of glucose as energy source, magnesium sulfate, which provides a source of magnesium ions for enzymatic reactions in DNA replication and $CaCl_2$. TB medium enables bacteria to maintain an extended growth phase, leading to enhanced biomass production. Glycerol acts as energy source, while tryptone and yeast extract provide growth factors and additional nutrients. Potassium phosphates stabilize pH, resulting in improved cell viability (Lessard, 2013). *E. coli* biomass production, based on OD_{600}, was determined after overnight growth at 37 °C, 250 rpm.

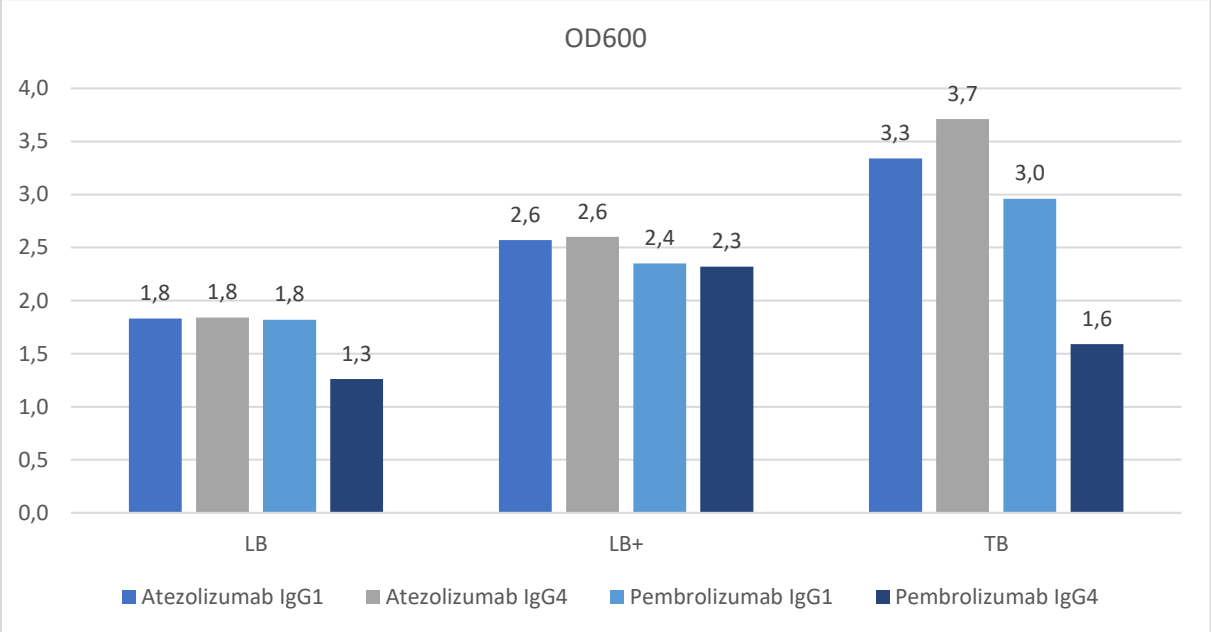

figure 10: Optical densities at an absorbance of 600 nm reveal *E. coli* biomass production in different growth media and having different plasmids incorporated. Plasmid isotypes: Atezolizumab IgG1 (pVITRO-Atezo-IgG1), Atezolizumab IgG4 (pVITRO-Atezo-IgG4), Pembrolizumab IgG1 (pVITRO-Pembro-IgG1), Pembrolizumab IgG4 (pVITRO-Pembro-IgG4).

Figure 10 shows that overall, supplemented LB medium (LB+) and TB medium lead to higher *E. coli* biomass production for all plasmid subtypes compared to growth in LB media. This finding is not surprising, since both LB+ and TB medium include supplementary substances,

which provide additional energy sources aimed to accelerate bacterial growth. For *E. coli* cells producing pVITRO-Atezo-IgG1 or -IgG4, as well as pVITRO-Pembro-IgG1, a clear trend of increasing OD_{600} values was found from growth in LB, followed by LB+ and TB medium. Cultivation in TB medium resulted in the highest biomass production for these cells. *E. coli* cells with the vector pVITRO-Pembro-IgG4 had the highest density following growth in LB+ medium, while there were no significant differences found between OD_{600} values obtained from LB or TB medium. In case of cells transfected with the pVITRO-Atezo-IgG1 plasmid, growth in TB medium resulted in a 1.8-fold increase compared to the standard LB medium and even more than 2-fold increase for pVITRO-Atezo-IgG4 in TB medium, compared to LB medium. Growth of *E. coli* cells producing pVITRO-Pembro-IgG1 was increased by 67 % from LB medium to TB medium, while for cells with pVITRO-Pembro-IgG4, an increase in biomass production of even 76 % was achieved comparing the lowest value in LB to the highest OD_{600} obtained from growth in LB+ medium.

4.1.1.2. Plasmid DNA isolation and concentration determination

In the next step, the correlation between *E. coli* biomass production and plasmid DNA yield obtained from different culture media was tested. Figure 11 provides an overview of the detected plasmid DNA concentrations, with the highest value of each plasmid isotype highlighted in red.

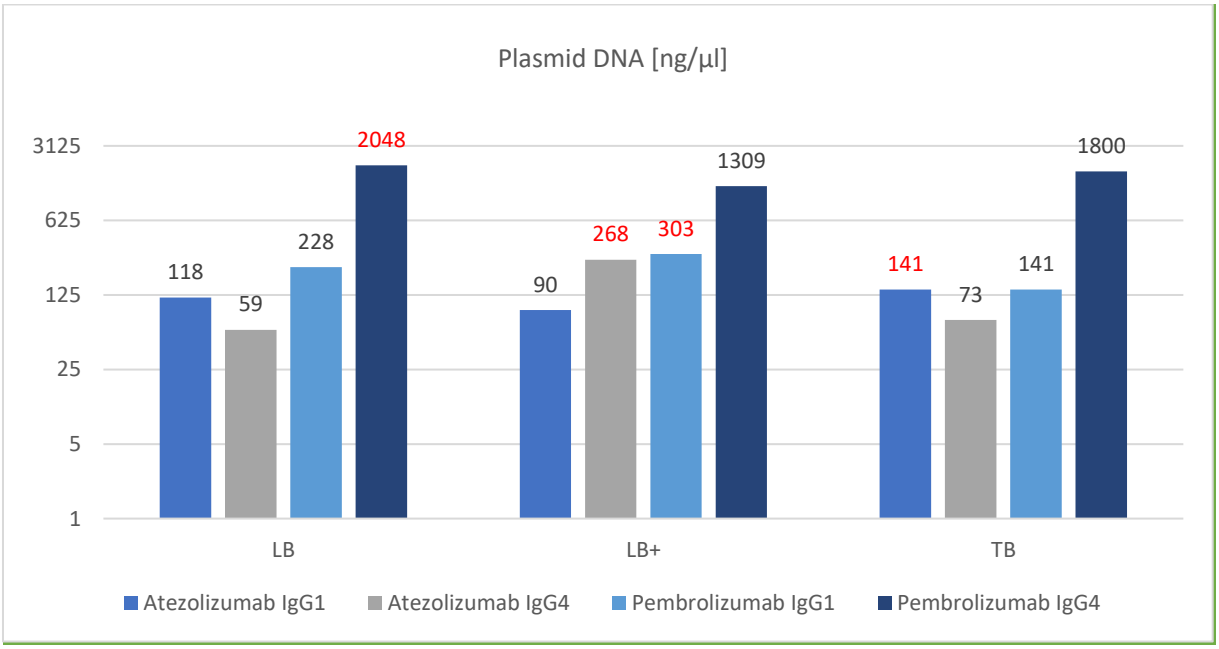

figure 11: Plasmid DNA concentrations [ng/µl] obtained from purification of *E. coli* cells grown in different culture media are shown. Plasmid isotypes: Atezolizumab IgG1 (pVITRO-Atezo-IgG1), Atezolizumab IgG4 (pVITRO-Atezo-IgG4), Pembrolizumab IgG1 (pVITRO-Pembro-IgG1), Pembrolizumab IgG4 (pVITRO-Pembro-IgG4).

Overall, there was no significant correlation observed between biomass production and plasmid DNA yield. In case of pVITRO-Atezo-IgG1, the highest plasmid DNA yield was achieved from growth in TB media (141 µg/ml), which correlates with the highest biomass production. However, biomass production and DNA yield did not match up for the other culture media. Plasmid yield was 1.3-fold higher from cells grown in LB media than in LB+ media, despite 1.4-fold higher cell density in LB+ media. For pVITRO-Atezo-IgG4, no significant differences were found between DNA concentrations obtained from growth in LB media and TB media, despite significant difference in biomass production. Plasmids derived from *E. coli* growth in LB+ media resulted in the highest DNA yield (268 µg/ml). LB+ media further lead to the highest yield of plasmid DNA for pVITRO-Pembro-IgG1, with up to 2-fold increase compared to TB or LB media, resulting in 303 µg/ml DNA. The highest plasmid DNA yield was achieved for pVITRO-Pembro-IgG4 (2048 µg/ml), with numbers 14 times higher compared to the lowest plasmid DNA yield achieved for pVITRO-Atezo-IgG1. Interestingly, growth in LB media resulted in the highest plasmid DNA yield, despite its low *E. coli* biomass production. However, DNA values achieved from purification of pVITRO-Pembro-IgG4 were significantly higher than the other plasmid isotypes in all growth media.

These results highlight the major impact of plasmid isotype produced by *E. coli* cells on the required culture conditions and growth of cells as well as plasmid yield. The results also suggest that plasmids have different copy-numbers. This explains why pVITRO-Atezo-IgG1 plasmid DNA isolated from the second highest *E. coli* cell density resulted in such low DNA concentrations, while for pVITRO-Pembro-IgG4 on the other hand, the highest DNA concentration was obtained from the overall lowest cell density. Too high density of cells can overload the purification column, interfering with proper DNA isolation. For the following experiments and plasmid production, LB media was chosen for the growth of cells with pVITRO-Pembro-IgG4, LB+ media was chosen for production of pVITRO-Atezo-IgG4 as well as pVITRO-Pembro-IgG1, while TB media was used for production of pVITRO-Atezo-IgG1. DNA purity was high for all isotypes and applied culture media, determined via A260/280 ratio *(table 6).*

table 6: Quality of plasmid DNA purified from *E. coli* cells in different culture media evaluated via A260/280 values.

	LB medium	LB+ medium	TB medium
	Average A260/280 ratio		
pVITRO-Atezo-IgG1	1.81	1.85	1.80
pVITRO-Atezo-IgG4	1.76	1.80	1.75
pVITRO-Pembro-IgG1	1.84	1.80	1.80
pVITRO-Pembro-IgG4	1.80	1.80	1.80

4.1.2. Plasmid production

E. coli biomass production after overnight growth was measured based on the OD_{600}, and the values were used for calculation of culture volume required for purification. According to the manufacturer, the use of a total cell mass of 160 is suggested for low copy plasmids, whereat cell mass equals OD_{600} x ml of culture (Sigma-Aldrich, 2015). For achievement of highest possible DNA concentrations, plasmids were considered as low copy plasmids, except for pVITRO-Pembro-IgG4, for which a total cell mass of 80 was used. Plasmid DNA concentrations and A260/280 ratios were measured before and after sterile filtration *(table 7 and 8).*

table 7: Plasmid DNA concentrations and A260/280 values obtained from Plasmid Midiprep before sterile filtration.

	Plasmid DNA (µg/ml)	Average A260/280 ratio
pVITRO-Atezo-IgG1	361	1.8
pVITRO-Atezo-IgG4	452	1.9
pVITRO-Pembro-IgG1	491	1.9
pVITRO-Pembro-IgG4	901	1.9

table 8: Plasmid DNA concentrations and A260/280 values from Plasmid Midiprep measured after sterile filtration through a 0.2 µm PES membrane.

	Plasmid DNA (µg/ml)	Average A260/280 ratio
pVITRO-Atezo-IgG1	272	1.8
pVITRO-Atezo-IgG4	339	1.9
pVITRO-Pembro-IgG1	412	1.9
pVITRO-Pembro-IgG4	765	1.9

Production of plasmid DNA was enhanced using different growth media for each recombinant *E. coli* strain, which were determined in the previous step. Using a Plasmid Midiprep system, volumes of up to 40 ml of cell culture were purified. Membrane sterilization of purified plasmid DNA was used to remove remaining impurities, which might interfere with eukaryotic transfection in the next step. Sterile filtration resulted in DNA loss of 25 % for plasmids containing human Atezolizumab and 15 % for pVITRO-Pembro-IgG1/4. However, plasmid DNA concentrations were suitable for subsequent transfections.

4.2. Plasmid DNA control assays

4.2.1. PCR and enzymatic digestion

4.2.1.1. PCR for amplification of plasmid heavy/ light chain sequences

Following amplification of plasmids in recombinant *E. coli* cells and purification via Plasmid Midiprep, PCR reactions were performed. These experiments aimed testing, whether the relevant DNA sequences encoding heavy and light chain sequences of the chimeric antibody were present in the purified plasmids. Primers for amplification of heavy chains were designed to anneal approximately 160 bp upstream from the start of the heavy chain sequence, including the signal peptide and the reverse primer annealed 60 bp downstream of the stop codon. Light chain regions were amplified similarly, with the forward primers annealing approximately 60 bp upstream from the start of the light chain sequence, including the signal peptide and reverse primers starting amplification 13 – 93 bp downstream of the stop codon of the light chain sequence. The amplified DNA fragments were then separated by 1.2 % agarose gel electrophoresis to examine the obtained DNA sizes. Table 9 provides an overview of the applied primer pairs and the expected DNA lengths in base pairs (bp). Using the software UGENE, annealing temperatures of the used primer pairs as well as expected DNA sizes were determined.

table 9: Overview of the applied primer pairs for amplification of plasmid DNA sequences encoding heavy or light chains of caninized mAbs and expected DNA lengths in bp.

Plasmid sequence	Primer pair	DNA plasmid	DNA length (bp)
heavy chain	Heavy chain 1 forward pCEP reverse	pVITRO-Atezo-IgG1	1565
		pVITRO-Atezo-IgG4	1564
		pVITRO-Pembro-IgG1	1570
		pVITRO-Pembro-IgG4	
light chain	Light chain 1 forward Light chain 2 reverse	pVITRO-Atezo-IgG1	735
		pVITRO-Atezo-IgG4	
		pVITRO-Pembro-IgG1	747
		pVITRO-Pembro-IgG4	
light chain	Light chain 1 forward RpVitro2	pVITRO-Atezo-IgG1	815
		pVITRO-Atezo-IgG4	
		pVITRO-Pembro-IgG1	827
		pVITRO-Pembro-IgG4	

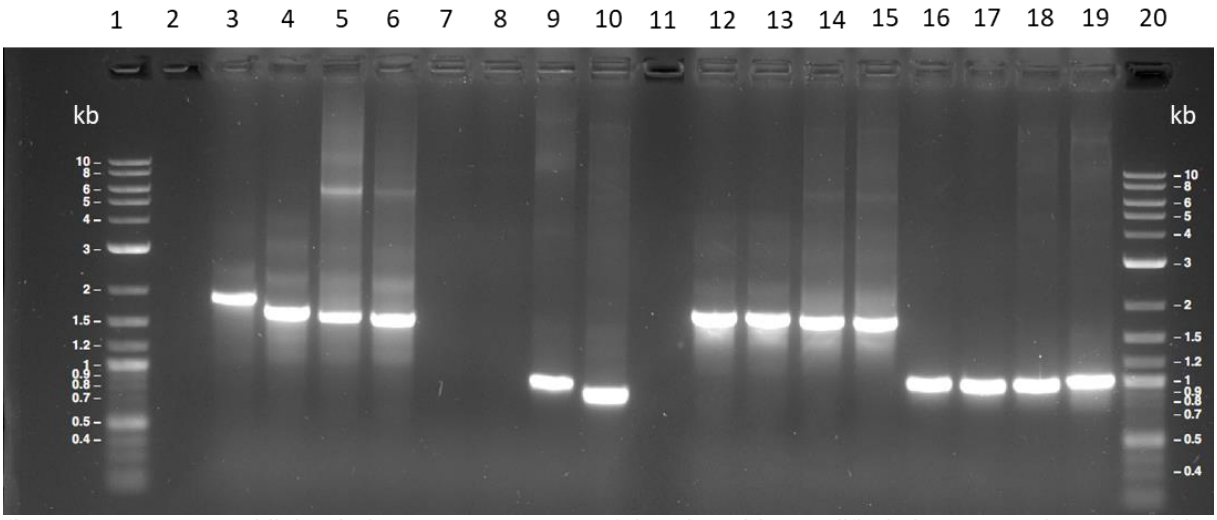

figure 12: Heavy and light chain DNA sequences of the plasmids amplified via PCR and separated by electrophoresis on a 1.2 % agarose gel. For amplification of heavy chain regions, the primers “Heavy chain 1 forward” and “pCEP reverse” were used (lane 3-6 and 12-15). Light chain sequences were amplified using the primers “Light chain 1 forward” and “Light chain 2 reverse” (lane 7- 10) and “Light chain 1 forward” in combination with “RpVitro2” (lane 16- 19). Loading of the gel was done according to table 10.

table 10: Amplification of plasmid DNA sequences via PCR with different primer pairs as listed. Loading of samples run on a 1.2% agarose gel, visualized in figure 12.

Lane	Sample	DNA sequence	Primer pair
1	DNA ladder	/	/
3/12	pVITRO-Atezo-IgG1	Heavy chain	Heavy chain 1 forward pCEP reverse
4/13	pVITRO-Atezo-IgG4		
5/14	pVITRO-Pembro-IgG1		
6/15	pVITRO-Pembro-IgG4		
7	pVITRO-Atezo-IgG1	Light chain	Light chain 1 forward Light chain 2 reverse
8	pVITRO-Atezo-IgG4		
9	pVITRO-Pembro-IgG1		
10	pVITRO-Pembro-IgG4		
16	pVITRO-Atezo-IgG1	Light chain	Light chain 1 forward RpVitro2
17	pVITRO-Atezo-IgG4		
18	pVITRO-Pembro-IgG1		
19	pVITRO-Pembro-IgG4		
20	DNA ladder	/	/

Two PCR reactions were conducted for amplification of heavy and light chain sequences of all plasmids. As visible on the agarose gel in figure 12, no PCR products were obtained for the light chain sequences of both pVITRO-hygro-Atezo-IgG1 and -IgG4, using the primers “Light chain 1 forward” and “Light chain 2 reverse” (see lanes 7 and 8). The absence of the PCR products might be due to insufficient annealing of primers or due to a mismatch in the DNA sequence in the location of primer annealing. Amplification of light chain sequences of Pembrolizumab IgG1 and IgG4 isotypes with the same primers resulted in correct-sized DNA bands (lanes 9 and 10). The light chain sequence of pVITRO-hygro-Pembro-IgG1 resulted in a slightly higher DNA band on the gel than its IgG4 counterpart. Due to the absence of PCR products obtained for light chain sequences of two plasmids, another reverse primer was applied in the second PCR run, aimed to amplify all light chain sequences, while the forward primer was maintained. “RpVitro2” annealed 50 bp downstream of the previous reverse primer. As visible on the agarose gel, amplification with the new primer pair lead to correct DNA bands for the light chain sequences of all plasmid isotypes. Amplification of heavy chain regions lead to size-specific DNA bands of all plasmids in both PCR reactions. Furthermore, additional larger, fainted DNA bands were found on the gel in almost every lane with sizes ranging from 2 - 8 kb, considered to be resulting from plasmid DNA fragments as well as full length plasmids remaining within the PCR reaction.

4.2.1.2. Enzymatic restriction digestion

To further examine the heavy and light chain sequences obtained via PCR from the produced plasmids, enzymatic digestion reactions were conducted, and the digested DNA fragments were separated on a 1.5 % agarose gel via electrophoresis, as depicted in figure 13. The restriction enzymes EcoRI-HF as well as BstXI were used. A restriction site for EcoRI-HF was present in the heavy chain sequence of all four plasmids, while BstXI recognizes a restriction site only in the light chain of pVITRO-Pembro-IgG1 and pVITRO-Pembro-IgG4. Table 11 summarizes the DNA lengths in bp expected from the enzymatic digestion reaction of the PCR products, while table 12 provides an overview of the loaded samples run on the agarose gel.

table 11: Enzymatic digestion of DNA fragments leads to characteristic DNA bands separated by electrophoresis on agarose gels. Primer pairs and restriction enzymes used for digestion of each DNA fragment are summarized. The DNA length in bp expected from enzymatic degradation was calculated using the software UGENE.

DNA region *Primer pair* Restriction enzyme	DNA plasmid	Restriction site	Expected DNA length (bp)
Heavy chain *Heavy chain 1 forward* *pCEP Reverse* EcoRI-HF	pVITRO-Atezo-IgG1	1	635, 925
	pVITRO-Atezo-IgG4		
	pVITRO-Pembro-IgG1	1	641, 925
	pVITRO-Pembro-IgG4		
Light chain *Light chain 1 forward* *Light chain 2 reverse* BstXI	pVITRO-Atezo-IgG1	No PCR products	/
	pVITRO-Atezo-IgG4		
	pVITRO-Pembro-IgG1	1	229, 514
	pVITRO-Pembro-IgG4		
Light chain *Light chain 1 forward* *RpVitro2* BstXI	pVITRO-Atezo-IgG1	No restriction site	815
	pVITRO-Atezo-IgG4		
	pVITRO-Pembro-IgG1	1	229, 594
	pVITRO-Pembro-IgG4		

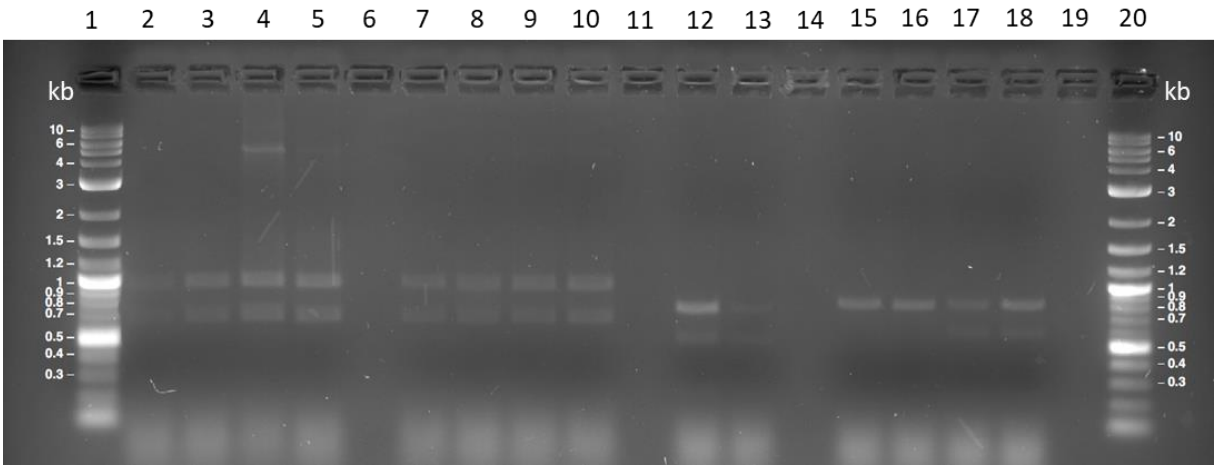

figure 13: Plasmid heavy and light chain DNA sequences were digested using two different restriction enzymes and separated by size on a 1.5 % agarose gel. Heavy chain DNA sequences were cut using the restriction enzyme EcoRI-HF (lanes 2-5 and 7-10 show samples from two different PCR runs). Light chain DNA fragments were degraded using the enzyme BstXI (lanes 12-13 with only pVITRO-Pembro-IgG1 and pVITRO-Pembro-IgG4 from the first PCR and all plasmid isotypes in lanes 15-19 from the second PCR). Loading of gel is summarized in table 12.

table 12: Enzymatic digestion of PCR-amplified heavy and light chain plasmid sequences, separated by electrophoresis. Loading of samples run on a 1.5 % agarose gel *(figure 13)*, DNA sequence and restriction enzymes used for digestion.

Lane	Sample	DNA sequence	Restriction enzyme
1	DNA ladder	/	/
2/7	pVITRO-Atezo-IgG1	Heavy chain	EcoRI-HF
3/8	pVITRO-Atezo-IgG4		
4/9	pVITRO-Pembro-IgG1		
5/10	pVITRO-Pembro-IgG4		
15	pVITRO-Atezo-IgG1	Light chain	BstXI
16	pVITRO-Atezo-IgG4		
12/17	pVITRO-Pembro-IgG1		
13/18	pVITRO-Pembro-IgG4		
20	DNA ladder	/	/

Enzymatic digestion was performed with all DNA fragments obtained from two previous PCR reactions and the agarose gel shows obtained DNA bands. Lanes 2-5 and 7-10 resulted from the digestion of heavy chain regions with the restriction enzyme EcoRI-HF, each leading to two bands with characteristic sizes, as calculated via the software UGENE. In lane 4, representing enzymatic restriction digestion of the heavy chain fragment of pVITRO-hygro-Pembro-IgG1 obtained from the first PCR reaction, an additional DNA band is visible having a size of approximately 6 kb. The same DNA band was already present in the

sample from the preceding PCR run (*figure 12, lane 6),* representing remains of plasmid DNA. Enzymatic digestion of light chain sequences of both IgG isotypes with Pembrolizumab resulted in each 2 bands (lanes 12, 13, 17, 18) with characteristic sizes. Light chain regions of p-Vitro-hygro-Atezo-IgG1/IgG4 had no restriction site for the enzyme BSTXI, resulting in one DNA band as expected at 815 bp, representing full length light chain DNA fragments.

4.2.2. Plasmid DNA sequencing and alignment via UGENE

DNA sequencing results were obtained from the company Eurofins. For sequencing, the company uses a technique termed cycle sequencing, which is a modification of the traditional Sanger sequencing method. Heavy and light chain sequences of each plasmid isotype were amplified. For amplification of each sequence, a forward, as well as a reverse primer, were used separately, resulting in two sequencing results per DNA region. By use of the software UGENE, obtained DNA sequences were aligned with the reference sequences. Figures 14 and 15 demonstrate parts of the alignment of obtained DNA sequences with the heavy and light chain sequences of the plasmid pVITRO-Atezo-IgG1. Color-coding of bases visualizes the identity of aligned sequences. Evenly separated, well-formed, distinctive single-colored peaks indicate successful sequencing results, resulting from absence of background signals and appropriate purity of DNA. These characteristics were found in both heavy and light chain regions of the shown sequence alignment

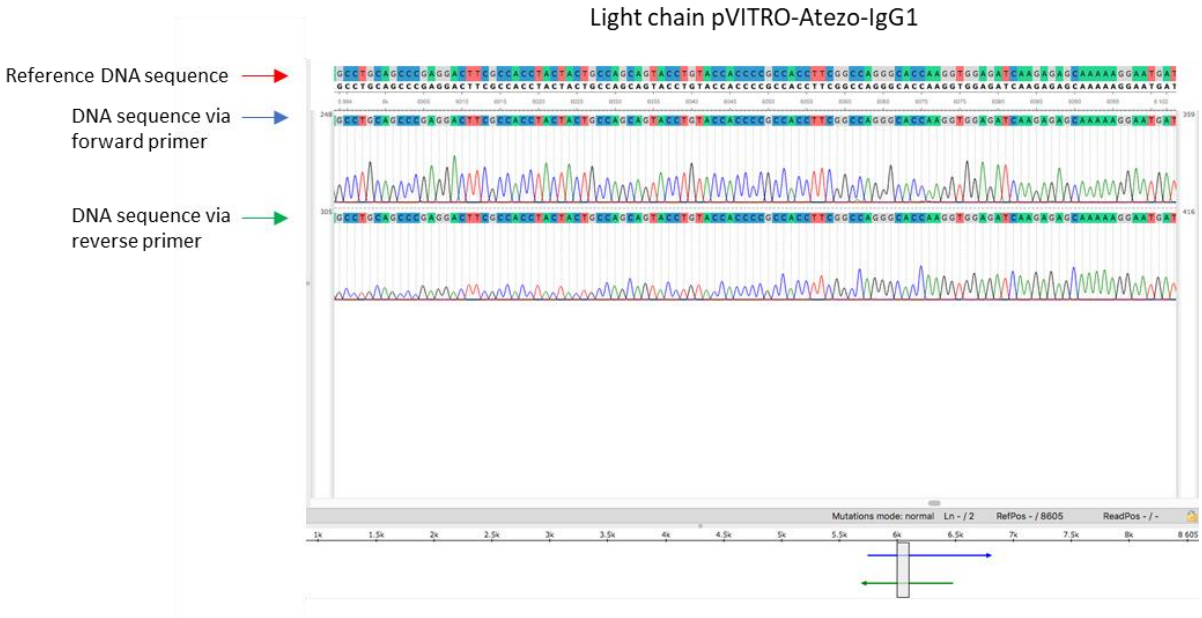

figure 14: DNA sequence alignment of the light chain regions of the plasmid pVITRO-Atezo-IgG1, undertaken via the software UGENE. DNA sequences obtained from amplification via a forward primer (indicated as blue arrow), and a reverse primer (indicated as green arrow) were aligned to the reference plasmid DNA sequence, constructed in silico.

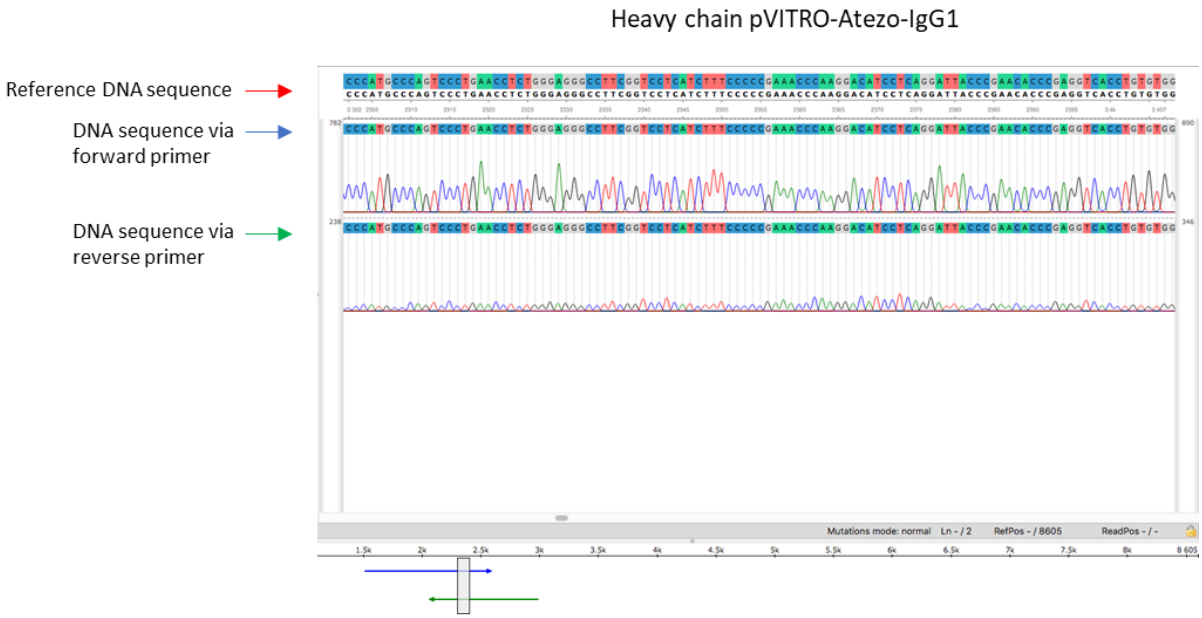

figure 15: DNA sequence alignment of the heavy chain regions of the plasmid pVITRO-Atezo-IgG1. Alignment of two DNA sequences, obtained from amplification via a forward primer (indicated as blue arrow) and a reverse primer (indicated as green arrow), to the reference plasmid DNA sequence, constructed in silico.

In case of all plasmids, alignments of DNA sequences encoding antibody heavy and light chains exhibited no changes in amino acids. It was further ensured, that stop codons were incorporated at the end of each gene. DNA sequencing results concurred highly with the constructed reference DNA sequences. Plasmids were therefore chosen for transfection of eukaryotic cells in the next step.

4.3. Expi293F cell maintenance and viability

Expi293F cells were cultured in Expi293F™ Expression Medium as recommended by the manufacturer. In parallel, cells were maintained in HyClone SFM4HEK293 media, which is optimized for high cell growth and recombinant protein production of human embryonic kidney (HEK) 293 cells. Expi293F cells originate from this cell line and are adapted to grow at high densities in suspension. The experiment was designed to determine the effect of growth media on the viability of Expi293F cells over a period of 4 weeks, subculturing cells twice per week. At each passaging step, cell viability was monitored. The aim of this experiment was to reduce costs for the cultivation of Expi293F cells without losing the cell viability. The goal was to mediate cell viability of ≥90 %. Figure 16 presents the results obtained from the measurements of cell viability.

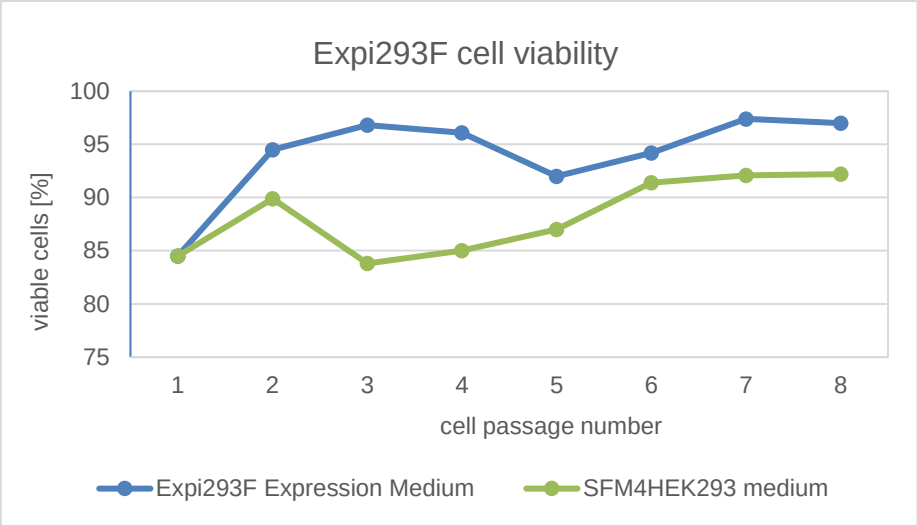

figure 16: Expi293F cell viability monitored over a period of 4 weeks in two different growth media, subculturing cells twice per week.

It is apparent from figure 16, that Expi293F cells cultured in Expi293F Expression medium recover faster after thawing and show higher viability overall compared to cells grown in SFM4HEK293 medium. At the time point of the first measurement, one day after thawing, cell viability of 85 % was measured in both growth media. According to the manufacturer of Expi293F cells, viability may drop to 80 % at 24 hours post-thaw but should not sink below 70 %. Within 4–7 days after thawing, viability should reach ≥90 % (Thermo Fisher, 2019). However, cell viability increased in both media, reaching 95 % in Expi293F Expression medium and 90 % in SFM4HEK293 media at the second measurement, 4 days after thawing. At the third cell passage, viability of cells grown in Expi293F Expression medium increased to 97 % before exhibiting a slight trend of decrease reaching the lowest value of 92 % at the fifth subculture, two weeks after thawing. Within the next three passages, cell viability rose, reaching 97% again. The trend of cell viability in SFM4HEK293 media dropped to the lowest value of 84 % after 8 days at the third passage, however, increased steadily over the following cell passages, reaching cell viability of 91- 92 % within the last three measurements. These results suggest that Expi293F cells grown in SFM4HEK293 media require more time to recover, however cell viability reached values of ≥90 %, sufficient for subculturing of cells. It was shown that Expi293F cells can alternatively be cultured in the cheaper medium, reducing costs tremendously.

4.4. Transfection and antibody harvest

Eukaryotic Expi293F cells were transfected with two different techniques. One transfection method was performed in suspension using the ExpiFectamine™ 293 Transfection Kit, while the other transfection method was undertaken adjusting Expi293F cells for adherent growth

and using the Lipofectamine LTX transfection kit. Caninized mAbs were termed “mAb-Atezo-IgG1”, “mAb-Atezo-IgG4”, “mAb-Pembro-IgG1” and “mAb-Pembro-IgG4”.

4.4.1. Transfection of eukaryotic Expi293F cells in suspension

The first applied transfection technique was in suspension, a process that takes only one week until antibody harvest. Several samples were purified via affinity chromatography, the results of which are summarized in the following. Production of mAbs was tested using dot blots, SDS-PAGEs and western blots.

4.4.1.1. Antibody purification via affinity chromatography

The mAbs were purified from the cell supernatant using affinity chromatography. Therefore, Protein A affinity columns were used. Protein A is a bacteria-derived protein that interacts with high affinity and specificity to the Fc region of IgG-class antibodies from multiple mammalian species such as humans and dogs. The 46.7 kDa protein has four high-affinity binding sites that target the Fc region. The ligand has a medium binding capacity for canine IgG, according to the manufacturer (GE Healthcare, 2009). A chromatogram resulting from the purification of mAb-Atezo-IgG1 is shown in figure 17. The column was equilibrated using PBS (pH 7.4) in the first step, followed by the application of supernatant. In the steps of Sample application, starting with fraction 1 (A/1), until the end of Column wash I, ending with fraction 5 (A/5), non-target proteins and other contaminants were washed off. This caused λ (280 nm) to rise and remain steady until the end of Column wash I, eluting contaminants by use of PBS (pH 7.4). Target proteins were eluted from the column by change of pH by applying 0.1 M citric acid (pH 2.7) gradually in the step of Elution I. Elution of mAb-Atezolizumab-IgG1 caused a peak at a wavelength of 280 nm in fraction 9, followed by another smaller peak emerging in fraction 11.

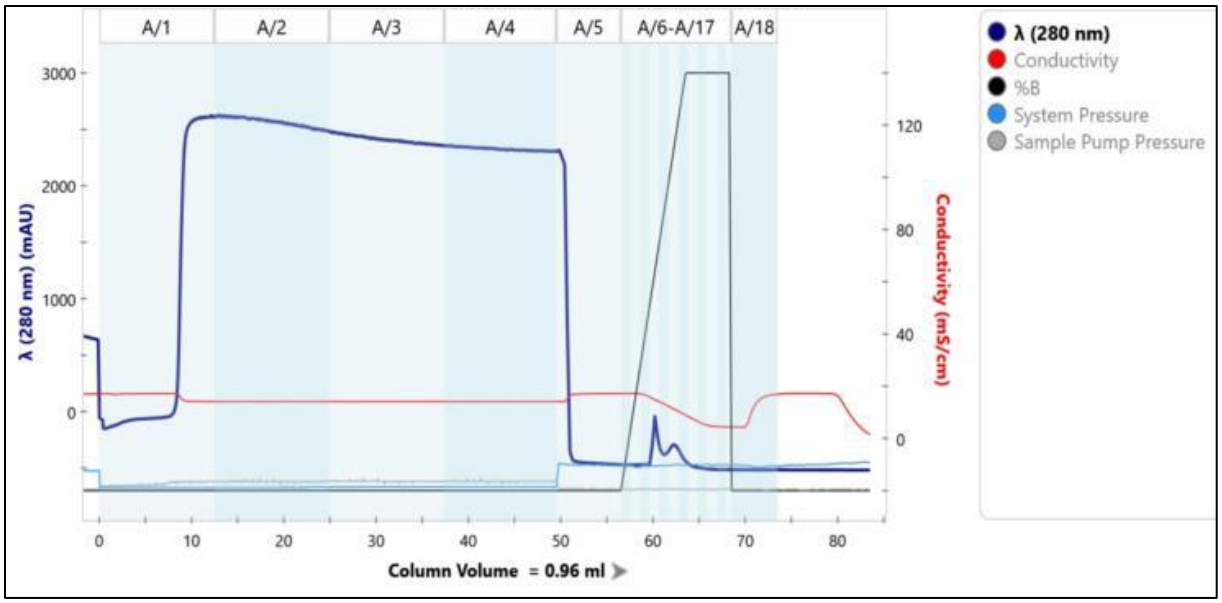

figure 17: Chromatogram from purification of caninized IgG1 anti-PD-L1 monoclonal antibodies (mAbs). Absorbance at a wavelength of 280 nm was measured, with a peak arising upon elution of target mAbs. Furthermore, conductivity, system and sample pressure were measured. %B describes gradual application of citric acid (pH 2.7), added to PBS for elution of target proteins.

4.4.1.2. SDS-PAGE and Silver staining

Samples purified via affinity chromatography were separated via SDS-PAGE at reducing and non-reducing conditions, visualizing protein bands via silver staining. Therefore, fractions obtained from affinity chromatography were used, in which a peak characteristic for the target protein was detected on the chromatogram. Full-length antibody was expected at a molecular weight of approximately 150 kDa for all antibody isotypes under non-reducing conditions, while reducing conditions lead to degradation of disulfide bonds. Separated heavy chain and light chains were expected at approximately 50 kDa and 25 kDa. Figure 18 shows two gels produced under non-reducing conditions. Samples from different transfections and following purifications were tested on the gels.

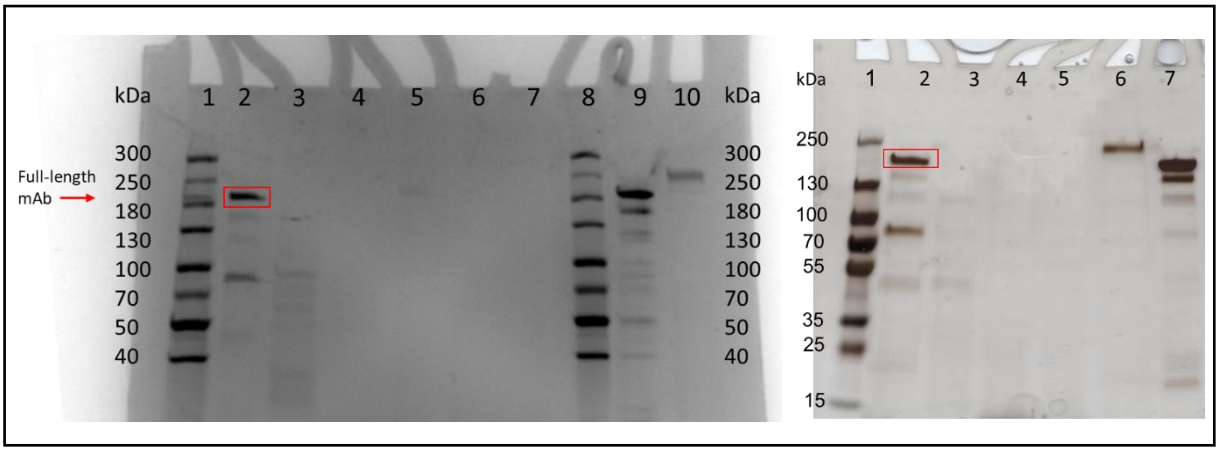

figure 18: Analysis of affinity-chromatography-purified mAbs on SDS-PAGE under non-reducing conditions (gel 1 on the left-hand side and gel 2 on the right-hand side), expecting full-length protein at 150 kDa. Human IgE (200 kDa) and Cetuximab, a chimeric human/ mouse anti-EGFR IgG1 mAb (145 kDa), were used as controls. Loading of gels was done as summarized in table 13. The red labelling indicates the purified full-length protein of mAb-Atezo-IgG1.

table 13: Sample labelling of non-reducing SDS PAGE visualized in figure 18, representing gel 1, depicted on the left-hand side and gel 2 on the right-hand side.

	Gel 1	Gel 2
Lane	Sample	Sample
1	Protein ladder (#26625)	Protein ladder (#26619)
2	mAb-Atezo-IgG1	mAb-Atezo-IgG1
3	mAb-Pembro-IgG1	mAb-Atezo-IgG4
4	mAb-Pembro-IgG1	mAb-Pembro-IgG1
5	mAb-Atezo-IgG1	mAb-Pembro-IgG4
6	mAb-Atezo-IgG4	Human IgE
7	mAb-Pembro-IgG1	Cetuximab (IgG1)
8	Protein ladder	
9	Cetuximab (IgG1)	
10	Human IgE	

It is apparent that protein bands resulting from purification of mAb-Atezo-IgG1 were detected on both gels in lane 2 under non-reducing conditions. Interestingly, on the left-hand sided SDS-PAGE, target antibody as well as positive controls resulted in protein bands of larger sizes than expected. Cetuximab, which is a chimeric human/ mouse IgG1 mAb targeting the epidermal growth factor receptor (EGFR), has an average molecular weight of 145 kDa, however was found at approximately 200 kDa, while human IgE, with a molecular weight of 200 kDa, resulted in a band at approximately 250 kDa. The largest protein band detected in the sample of purified mAb-Atez-IgG1 exhibited the same size as Cetuximab, suggesting that

proteins were similar in size, resembling full-length protein. Heterogeneities in molecular weights obtained on the SDS-PAGE might appear due to differences in the glycosylation of the antibodies. Furthermore, protein bands of IgG antibody subclasses might be unexpectedly larger using non-reducing conditions. The observed size heterogeneity might be minimized or eliminated upon usage of lower temperatures and addition of several alcohols (Kirley et al., 2018). Additional fainted protein bands were found on the gel 1 in lane two at sizes between 45- 180 kDa, as well as one stronger band between 70 and 100 kDa, considered to be resulting from antibody homodimers at 75 kDa. The second SDS-PAGE on the right-hand side in figure 18 shows similar results, with mAb-Atezo-IgG1 resulting in one sharp band at approximately 150 kDa, various unspecific fainted protein bands and one stronger band at approximately 75 kDa. The unspecific protein bands on both gels might result from incompletely produced and non-assembled parts of antibodies. One weak band resulting from another purification of mAb-Atezo-IgG1 was further found in lane 5 of the gel 1, resembling full-length antibody. For mAb-Pembro-IgG1, unspecific weak protein bands were found on the same gel, while no bands were detected on the second SDS-PAGE. Various protein bands were found for mAb-Atezo-IgG4, on the gel 2, however, no band resulted in the size resembling full-length antibody. On neither of the gels, mAb-Pembro-IgG4 was found. Figure 19 shows mAbs separated on an SDS-PAGE under reducing conditions.

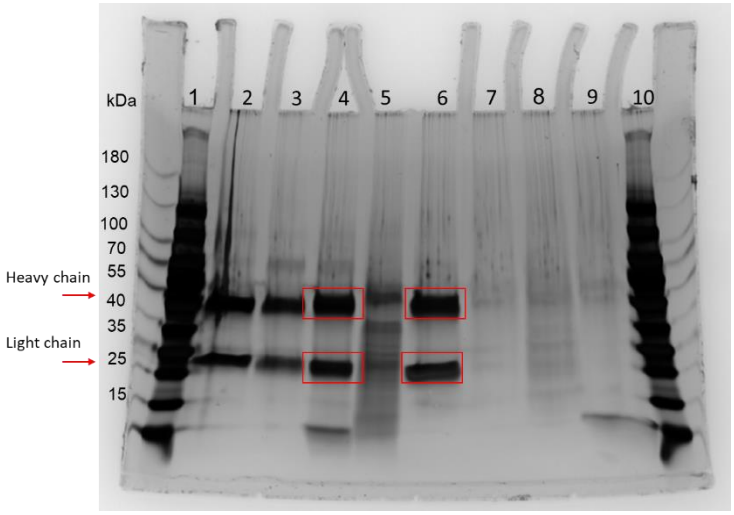

figure 19: Analysis of protein samples purified via affinity chromatography run on an SDS-PAGE under reducing conditions, expecting protein bands at 50 kDa and 25 kDa, resembling antibody heavy and light chains. Silver staining was used for protein detection. Cetuximab in lane 2 and canine total IgG in lane 3 served as controls. Loading of gel was done as listed in table 14 below. The red labelling indicates the purified and separated heavy and light chains of mAb-Atezo-IgG1.

table 14: Sample labelling of SDS page in figure 19 produced under reducing conditions.

Lane	Sample
1	Protein ladder (#26616)
2	Cetuximab (IgG1)
3	Canine total IgG
4	mAb-Atezo-IgG1
5	mAb-Atezo-IgG4
6	mAb-Atezo-IgG1
7	mAb-Atezo-IgG4
8	mAb-Pembro-IgG1
9	mAb-Pembro-IgG4
10	Protein ladder

From the SDS-PAGE in figure 19, it is apparent that protein bands, as well as background, are stained massively, probably resulting from too long staining by silver nitrate. Samples from two different purifications were applied for mAb-Atezo-IgG1 and -IgG4 in lanes 4- 7. From the gel it is apparent that mAb-Atezo-IgG1 in lanes 4, as well as 6, resulted in two strong protein bands at approximately 50 kDa and 25 kDa, as expected for antibody heavy and light chains. For mAb-Atezo-IgG4 in lane 5, size specific protein bands are apparent, giving a stronger signal than the multiple unspecific protein bands, which result in a blurry pattern. For the other antibody isotypes, no clear size-characteristic protein bands were found. Taken together, the results from SDS-PAGE and silver staining suggest that production and purification of mAb-Atezo-IgG1 worked properly, leading to size-characteristic protein bands under reducing as well as non-reducing conditions. The identity of protein bands was further validated using western blots (see Results 4.4.1.4.). The absence of size-specific protein bands for the other antibody isotypes suggested that there were issues either in the step of transfection and antibody production or in the purification step. Further analysis was required to determine the limiting step.

4.4.1.3. Dot blot

As compared to SDS-PAGE, dot blots are useful to analyze the antigenicity of the native recombinant proteins. Dot blots were thus prepared to detect the caninized mAbs using an anti-canine Horseradish peroxidase (HRP) conjugated IgG antibody derived from rabbit origin. The antibody targets the Fc region of canine IgG heavy chain. To evaluate the process of antibody harvest, a dot blot was undertaken with samples after each centrifugation step (see Methods 3.5.3.), as visualized in figure 20. In parallel to the procedure of antibody harvest

including three centrifugation steps, a 2-step centrifugation procedure was tested *(table 15),* comparing gained antibody concentrations on the blot. The dot blot was undertaken with two antibody isotypes, mAb-Atezo-IgG4 and mAb-Pembro-IgG4. Samples were applied twice.

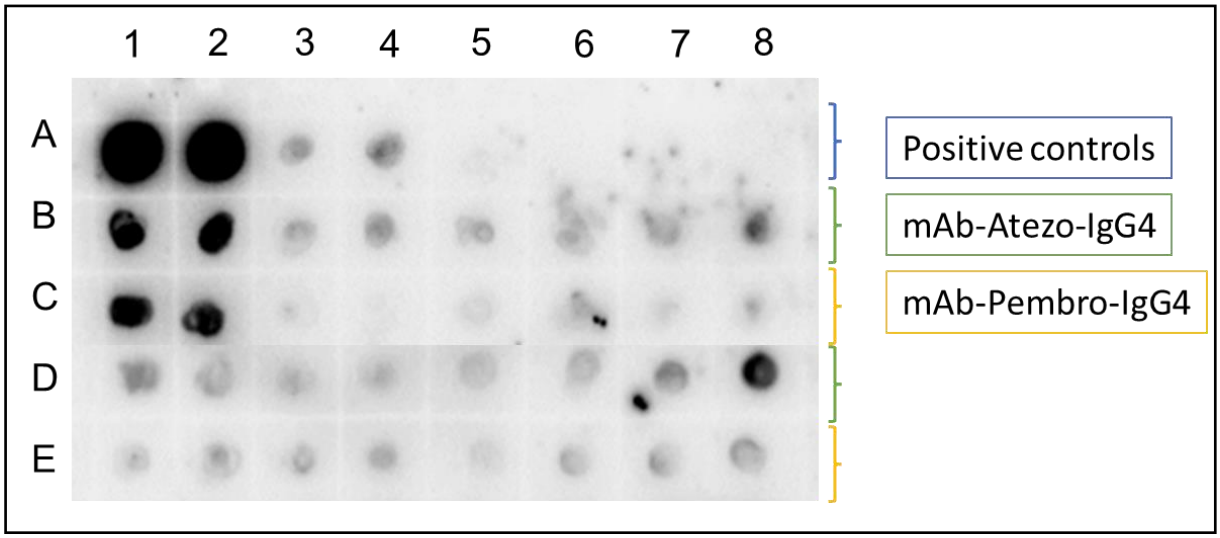

figure 20: Dot blot analyzing antibody concentration from transfected Expi293F cells after one week of mAb production. Evaluation of antibody harvest until purification, taking into consideration the centrifugation steps performed upon antibody harvest. Caninized mAbs were detected using an anti-dog IgG antibody and positive controls were canine total IgG and canine IgG3.

table 15: Labelling of the dot blot in figure 20, with antibody samples obtained from transfected Expi293F cells, monitoring antibody concentration throughout the centrifugation steps for removal of cell components. Two different centrifugation procedures were applied, visualized in blue and green color.

	1/2	3/4	5/6	7/8
A	Canine total IgG (10 mg/ml)	Anti-EGFR chimeric canine IgG3 mAb (0.4 mg/ml)	/	/
B/C	Expi293F cell culture one week after transfection	Supernatant after first centrifugation (280 x g, 7 min, RT)	Supernatant after second centrifugation (280 x g, 7 min, RT)	Supernatant after third centrifugation (20 000 x g, 30 min, 4 °C)
D/E	Supernatant after first centrifugation (1000 x g, 5 min, RT)	Supernatant after second centrifugation (14 000 x g, 10 min, RT)	Supernatant after third centrifugation (20 000 x g, 30 min, 4 °C) with protease-inhibitor and sodium azide	Supernatant after second centrifugation (14 000 x g, 10 min, RT) with protease-inhibitor and sodium azide

It is apparent from the dot blot that mAbs in the supernatant before centrifugation lead to high signals detected via chemiluminescence. However, antibody concentration in the supernatant was reduced substantially after the first centrifugation step of both centrifugation procedures

and both tested mAbs. The following centrifugation steps did not reduce antibody concentration significantly. Comparing antibody concentrations between the two centrifugation procedures detected on the blot lead to similar results, with the 2-step process resulting in slightly stronger signals particularly for mAb-Pembro-IgG4. Centrifugation steps were applied to remove any cell components before purification via affinity chromatography, with mAbs aimed to remain in the supernatant after centrifugation. Surprisingly, huge amounts of antibody were trapped within the cell pellet after centrifugation. Therefore, on another nitrocellulose blot *(figure 21),* the cell pellets of mAb-Atezo-IgG4, obtained after each centrifugation step, were applied, using samples from another transfection.

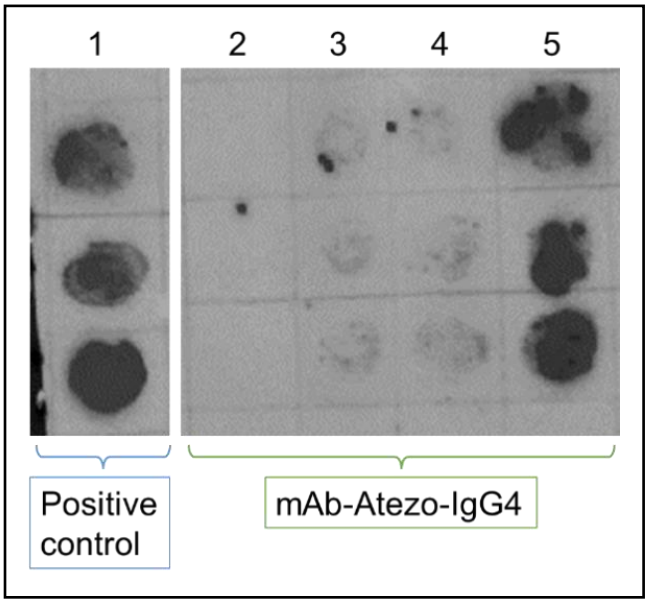

figure 21: Dot blot analyzing caninized mAb concentrations in cell pellets after each centrifugation step (column 3-5) and in the supernatant of transfected Expi293F cells after one week of production (column 2) with the isotype mAb-Atezo-IgG4. Canine total IgG (4 mg/ml) served as positive control (column 1).

Samples were applied in triplets (from top to bottom) as follows: Cell culture one week after transfection, cell pellet after the first centrifugation (280 x g, 7 min), cell pellet after the second centrifugation (280 x g, 7 min), cell pellet after the third centrifugation (20 000 x g, 30 min). As apparent from figure 21, the intensity of dots detected on the blot increased after each centrifugation step, leading to the strongest signals after the third centrifugation step, while surprisingly the concentration of mAbs in the supernatant was too low to be detected. These results suggest that significant amounts of antibody may remain within the cell pellet. On the same nitrocellulose blot, samples obtained from purified fractions of mAb-Atezo-IgG1 and mAb-Pembro-IgG4 *(figure 22)* were tested in parallel. Small amounts of antibodies were detected for both mAb isotypes.

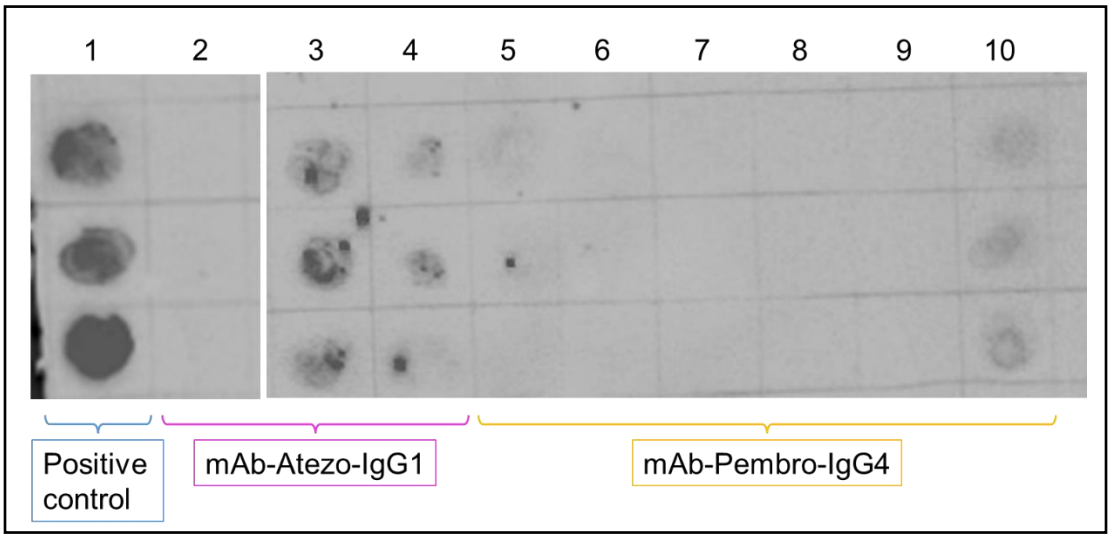

figure 22: Dot blot reveals caninized mAb concentrations in the supernatant of Expi293F cells one week after transfection (column 2 and 5) and purified fractions after affinity chromatography (column 3,4 and 6-10). Canine total IgG was used as positive control (column 1).

Samples were applied to the dot blot in triplets (from top to bottom) with cell culture before harvest (column 2 and 5) and purified samples from affinity chromatography (column 3 and 4 for mAb-Atezo-IgG1 and column 6- 10 for mAb-Pembro-IgG4). In both fractions collected from purification of mAb-Atezo-IgG1, antibodies were detected, while the concentration in the supernatant was too low for detection. For mAb-Pembro-IgG4, low mAb concentrations were detected in the supernatant, while in the purified fraction applied to line 10, stronger signals were obtained. However, mAb concentrations in all samples were rather low, requiring further analysis. To summarize, dot blot analysis revealed mAbs in the cell culture of Expi293F cells of all isotypes, after one week of growth, with mAb concentrations varying between antibody isotypes. Caninized mAbs were further found in the purified fractions after affinity chromatography, however, significant concentrations were also detected remaining within the cell pellet after centrifugation, suggesting that mAbs were partly trapped on or in the cells.

4.4.1.4. Western blot

Western blot analyses were performed with affinity-purified and dialyzed samples detecting caninized mAbs via an anti-dog IgG HRP conjugated antibody, which targets the Fc region of canine gamma heavy domains. Samples from different transfections were applied. Under reducing as well as non-reducing conditions, mAb-Atezo-IgG1 was the only antibody detected, visible in lane 4 and 6 of both blots *(figure 23 and 24)*. Expected protein sizes were 150 kDa for full length antibody and 50 kDa as well as 25 kDa for heavy and light chain regions, separated via reducing conditions. Protein bands found on the blot at non-reducing conditions were slightly larger, detected at approximately 180 kDa *(figure 23),* however also positive controls were found at larger sizes. In lane 4 of the same blot, a second band at 75 kDa was detected, considered to stem from antibody homodimers. Protein bands revealed under

reducing conditions *(figure 24)* resulted in sizes of approximately 50 kDa and 25 kDa for mAb-Atezo-IgG1 in lane 4 and 6.

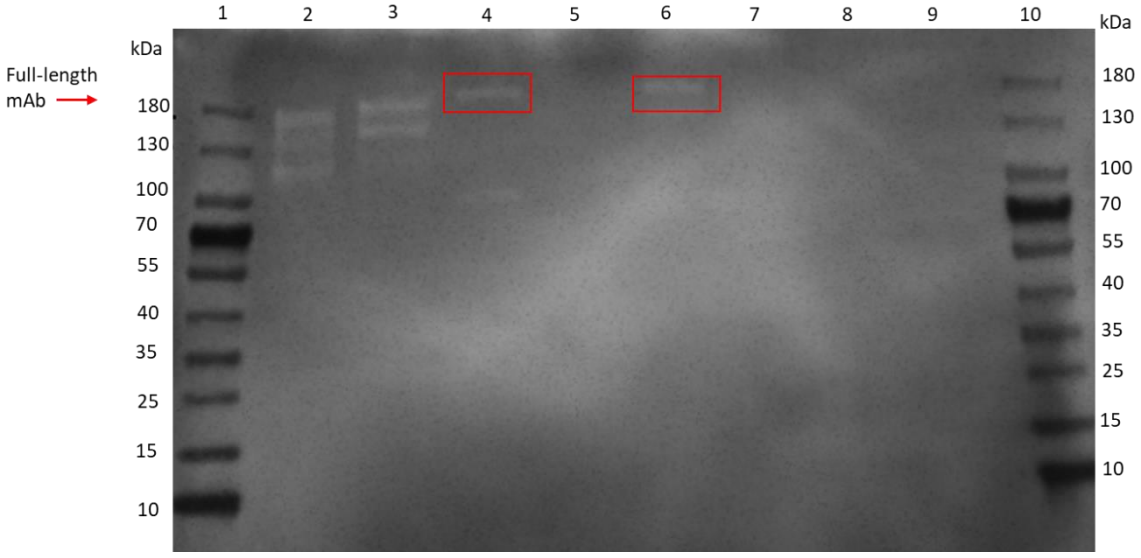

figure 23: Western blot produced under non-reducing conditions with caninized mAbs purified via affinity chromatography, revealed using an anti-dog IgG antibody from rabbit origin. Canine total IgG and anti-EGFR IgG1 were used as positive controls in lanes 2 and 3. Positive results were obtained for mAb-Atezo-IgG1 in lanes 4 and 6, as indicated in red. Loading of samples is listed in table 16.

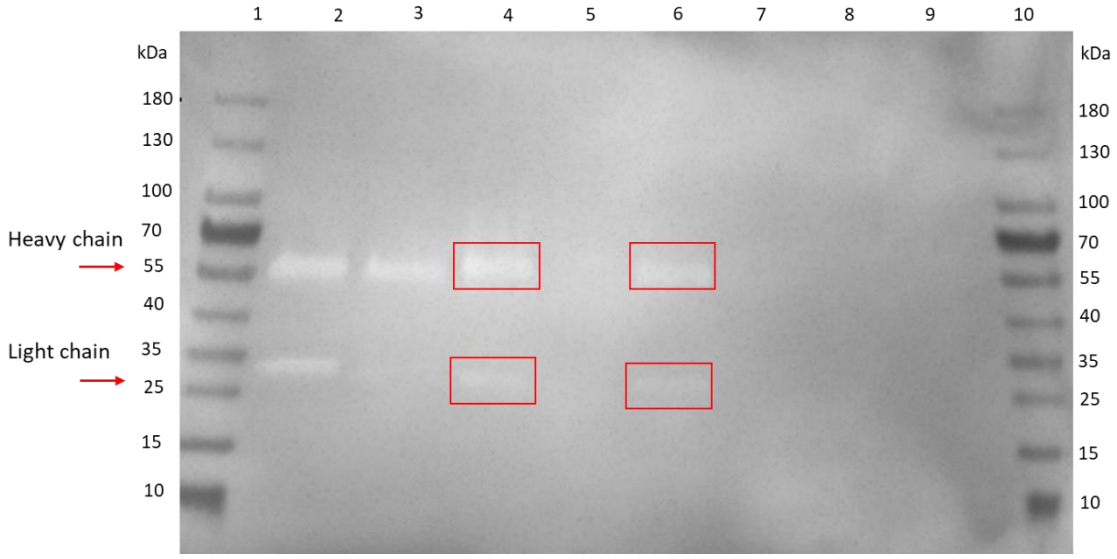

figure 24: Western blot produced under reducing conditions with mAbs purified via affinity chromatography, revealed using an anti-dog IgG antibody from rabbit origin. Canine total IgG and anti-EGFR IgG1 were used as positive controls in lanes 2 and 3. Heavy and light chain protein bands were obtained for mAb-Atezo-IgG1 in lanes 4 and 6, as visualized in red labelling. See plan of sample loading in table 16.

table 16: Sample labelling of Western blots from figures 23 and 24.

Lane	Sample
1	Protein ladder (#26616)
2	Cetuximab (anti-EGFR IgG1)
3	Canine total IgG
4	mAb-Atezo-IgG1
5	mAb-Atezo-IgG4
6	mAb-Atezo-IgG1
7	mAb-Atezo-IgG4
8	mAb-Pembro-IgG1
9	mAb-Pembro-IgG4
10	Protein ladder

The other antibody isotypes were not found separated on the Immunoblot. Further analysis was required to evaluate the limiting step of mAb establishment. We hypothesized that antibody production might be limited due to incorrect assembly and folding of antibodies. Assuming disulfide bond formation did not work properly, leading to formation of inclusion bodies, is one explanation why antibodies were not detected on the gel. Inclusion bodies might get stuck on the top of the SDS-PAGE, not being able to enter the gel. Our hypothesis based on the results obtained from dot blot analysis, that mAbs might be trapped on/in the expressing Expi293F cells, was further evaluated in the step of flow cytometric analysis (see Results 4.5.2.).

4.4.2. Transfection of adherent eukaryotic Expi293F cells

Our previous results from transfection were limited to production of caninized IgG1 anti-PD-L1 mAb, revealing correct sizes in SDS-PAGEs and Immunoblots under reducing as well as non-reducing conditions. We aimed to test another transfection strategy, in which cells were selected for integration of plasmid, increasing the number of positively transfected Expi293F cells. Cells were adapted to grow in adherence conditions using supplemented DMEM medium, leading to 90 % confluence upon transfection and positive clones were selected using hygromycin B. After two times of selection with hygromycin B, nine days after transfection, all cells from the mock transfection were detached and dead *(figure 25),* while non-treated cells from the mock transfection remained adherent *(figure 26),* showing that hygromycin B was responsible for killing cells without plasmid incorporated. No difference in viability was observed between the different concentrations of hygromycin B (50, 100, 200 µg/ml) added to the growth medium neither for the mock transfection nor for the normal transfections.

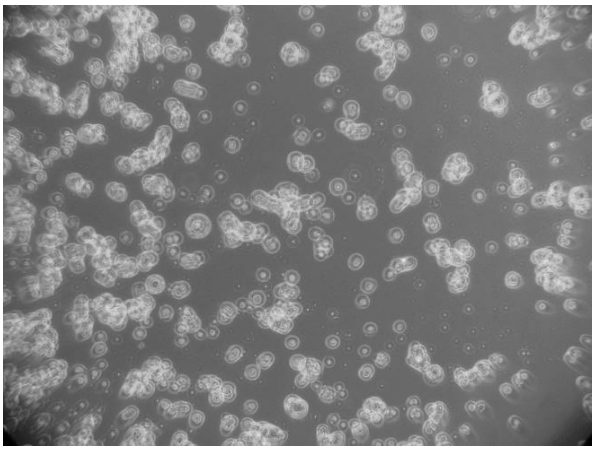

figure 26: Cells from mock transfection treated with 200 µg/ml hygromycin B are detached and die.

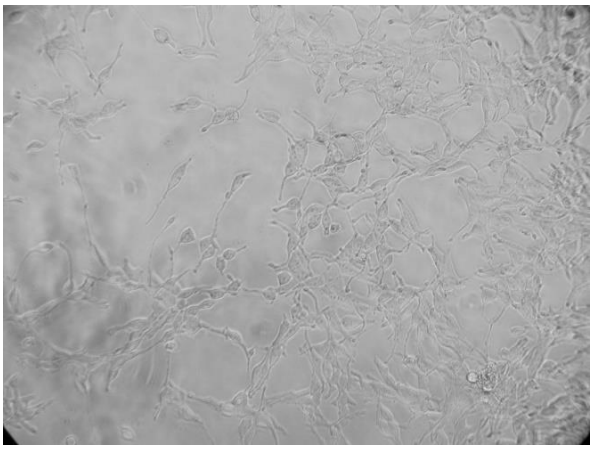

figure 25: Expi293F cell control group of untreated mock transfection remained adherent.

Expi293F cells showed different behavior upon transfection with the different plasmid isotypes. Cells transfected with plasmids containing canine IgG1 in combination with either human anti-PD-1 or anti-PD-L1 grew stably, forming a dense network after treatment with selection agent. However, cells transfected with plasmids with IgG4 isotype grew less stable. Loosely packed adherent colonies resulted from transfection with pVITRO-Pembro-IgG4. Cells transfected with pVITRO-Atezo-IgG4 resulted in cell death for all colonies in all wells over the period of hygromycin B selection. Figure 27 shows a microscopy picture of cells transfected with pVITRO-Atezo-IgG1, growing similar to cells transfected with pVITRO-Pembro-IgG1, while in figure 28, cells transfected with pVITRO-Pembro-IgG4 are depicted. Both pictures were taken 3 days after the second hygromycin B selection, meaning 9 days after transfection.

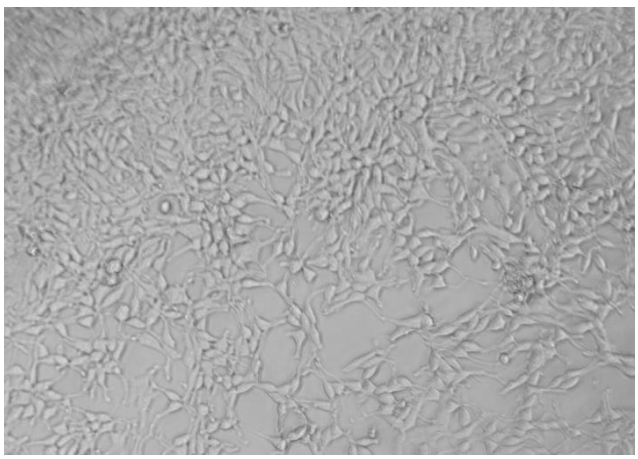

figure 27: Expi293F cells transfected with pVITRO-Atezo-IgG1 resulted in a densely packed network of adherent cells. Picture taken 9 days after transfection.

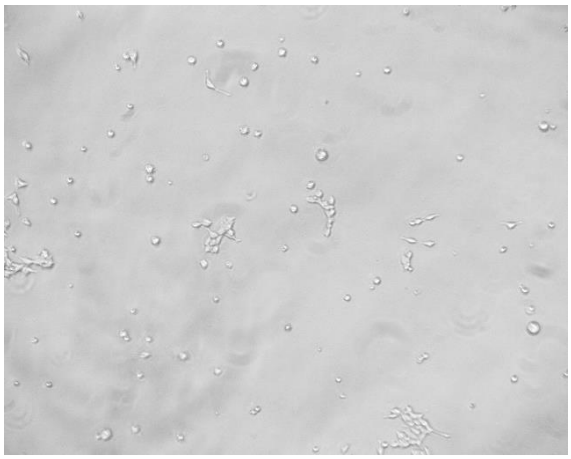

figure 28: Expi293F cells transfected with pVITRO-Pembro-IgG4 resulted in low confluency of cells. Picture taken 9 days after transfection.

A set of Expi293F cells expressing mAb-Atezo-IgG1, mAb-Pembro-IgG1 and -IgG4 were frozen and thawed after 2 weeks, resulting in adherent growth for all isotypes. All cells were resistant to the treatment with hygromycin B, suggesting that the freezing process did not harm the incorporation of plasmids within transfected cells. In parallel, positive clones of mAb-Atezo-IgG1, mAb-Pembro-IgG1 and -IgG4 were expanded to suspension and mAbs were harvested following one week of growth. Due to time limitations and the results from flow cytometric analysis, performed in parallel (see Results 4.5.2.), mAbs were not purified within this project.

4.4.3. Conclusion on transfection techniques

Two different approaches for transfection of eukaryotic Expi293F cells were applied. The Expi293™ Expression System is convenient for rapid production of proteins, taking into consideration that the transfection until harvest of proteins takes only one week. According to the manufacturer, this system leads to stable production of high yields of protein, which is a major advance (Thermo Fisher, 2019). However, using the Expi293™ Expression System resulted in production of limited amounts of caninized mAbs. Even though mAbs of all isotypes were detected in the supernatant of mAb-producing cells, it was shown on a dot blot *(figure 20)* that antibody concentration decreased substantially following centrifugation of cell culture. We hypothesized that mAbs were largely trapped on/in the expressing Expi293F cells, resulting in a lower concentration remaining in the supernatant. Antibodies were further detected in the cell pellet after centrifugation, revealed via a dot blot. Further investigations were suggested to gain more insight in reasons and solutions of this rate-limiting step. Transfection of adherent Expi293F cells was more time-consuming, taking up to three weeks until cells were adapted for growth in suspension again, required for the production of higher yields of mAbs. However, one advantage is the pre-selection with hygromycin B, before expansion to solution, which ensures that only clones that have the plasmid incorporated are used and expanded. The results of both transfection approaches suggested that expression of the IgG4 class antibodies was rather problematic than production of the IgG1 class antibodies. An issue to take into consideration might be improper folding of antibodies. The transfection techniques should be further compared concerning the yield of mAbs after purification in future steps, after having determined the rate-limiting step of mAb expression.

4.5. Flow cytometric analysis: Determination of binding capacity

4.5.1. Flow cytometric analysis of canine cancer cells

Binding affinities of human anti-PD-1 (Pembrolizumab) and anti-PD-L1 (Atezolizumab) mAbs chosen for construction of caninized mAbs were tested in three different canine cancer cell

lines. This experiment aimed at determining expression of PD-1 and PD-L1 by canine cancer cells and further identification of binding capacity of human anti-PD-1 and anti-PD-L1 to the canine checkpoint molecules produced by various cancer cell lines. Canine mammary carcinoma cell lines CF33, CF41 and canine osteosarcoma cell line D-17 were chosen for flow cytometric analyses. A geometric mean fluorescent intensity (MFI) value of ≥150 in APC was considered significant.

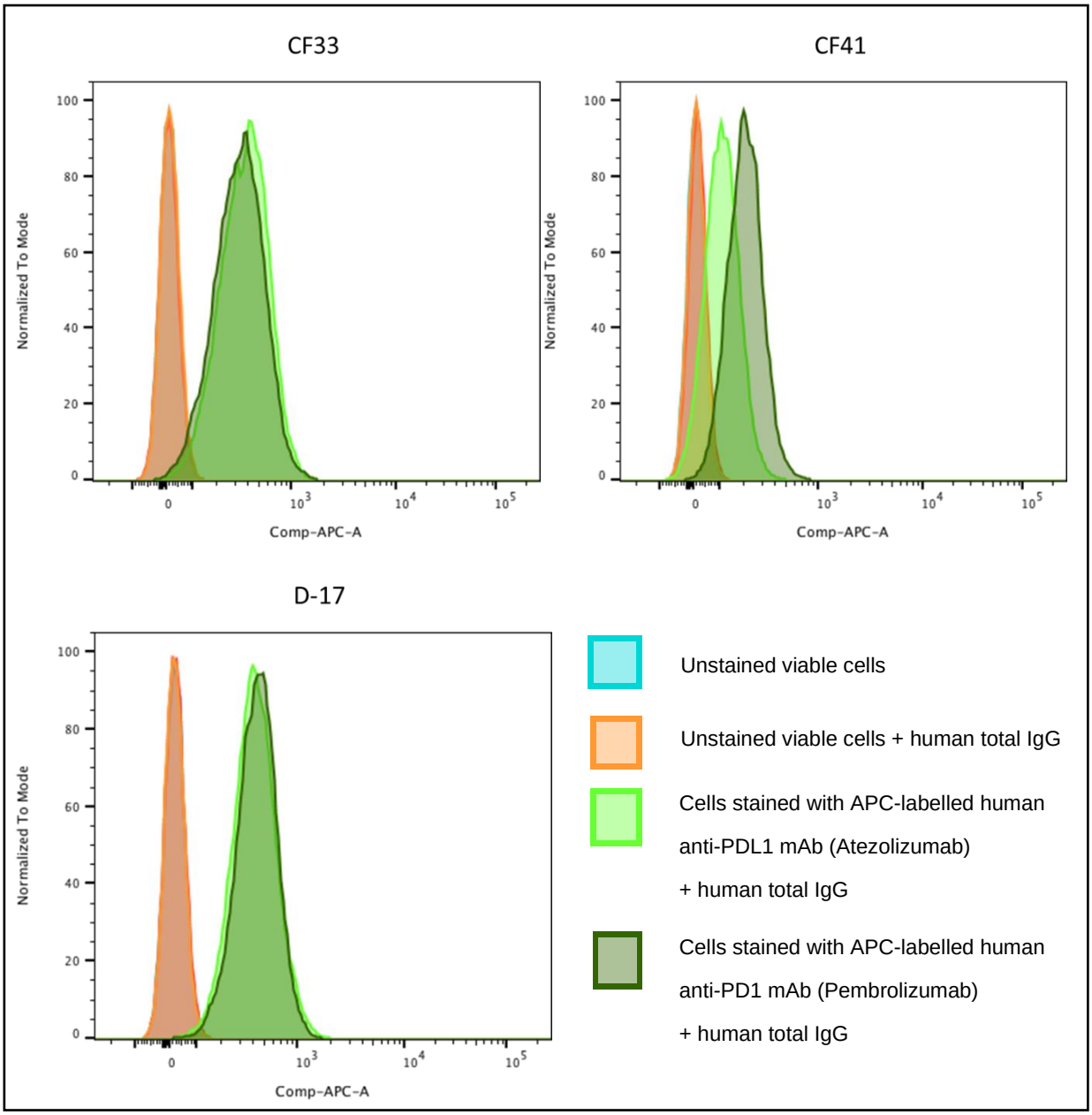

figure 29: Flow cytometric analysis evaluating the binding affinities of human APC-labeled anti-PD-1 (Pembrolizumab) and anti-PD-L1 (Atezolizumab) mAbs to the canine cancer cell lines CF41, CF33 and D-17. The geometric mean fluorescent intensity (MFI) in APC is visualized as graph.

table 17: Results from flow cytometric analysis detecting the binding capacities of human APC-labeled anti-PD-1 and anti-PD-L1 mAbs to the canine cancer cell lines CF33, CF41 and D-17, evaluated by determination of MFI (APC) values via the software FlowJo™, version 10.

	MFI (APC)		
	CF33	CF41	D-17
Unstained viable cells	24	23	31
Unstained viable cells + human total IgG	26	23	30
Cells stained with APC-labelled human anti-PDL1 mAb (Atezolizumab) + human total IgG	369	113	413
Cells stained with APC-labelled human anti-PD1 mAb (Pembrolizumab) + human total IgG	333	210	433

Binding of APC-labelled human mAbs resulted in a significant increase in MFI (APC) from unstained to cells stained with human anti-PD-1 and anti-PD-L1 APC-labeled mAbs for all cancer cell lines. Only the binding of human PD-L1 to canine CF41 cells did not lead to a significant increase, resulting in MFI (APC)= 113. Anti-PD-1 resulted in a significant increase of APC signal for all cancer cell lines, with the highest MFI (APC) values for D-17 cells, with MFI (APC)= 433. The binding capacity of APC-labelled anti-PD-L1 was also highest for D-17 cells with MFI (APC) values of 413. These results suggest that the tested canine mammary carcinoma cell lines and canine osteosarcoma cell lines express checkpoint molecules on their surface, proposing that potentially caninized mAbs in the future may be used for treatment of these tumour types.

4.5.2. Flow cytometric analysis of human Expi293F cells

Another aim of flow cytometric analysis was to test the binding of human Atezolizumab and Pembrolizumab against the human expression cell line Expi293F. Due to the low concentration of caninized mAbs found in the supernatant of transfected cells, we hypothesized that mAbs may be trapped on the surface of expressing cells, which was also in line with results found from the dot blot *(figure 20)*, showing that antibody concentration in the supernatant was reduced substantially after centrifugation of cells. Therefore, we aimed to test if Expi293F cells produce checkpoint molecules PD-1 and PD-L1 on their surface. Expression of checkpoint molecules on their surface may result in the binding of caninized mAbs and further might lead to downregulation of gene expression, taking into consideration the inhibitory properties of

PD-1 and PD-L1. For this experiment, cells transfected with pVITRO-Pembro-IgG1 as well as non-transfected Expi293F cells were tested.

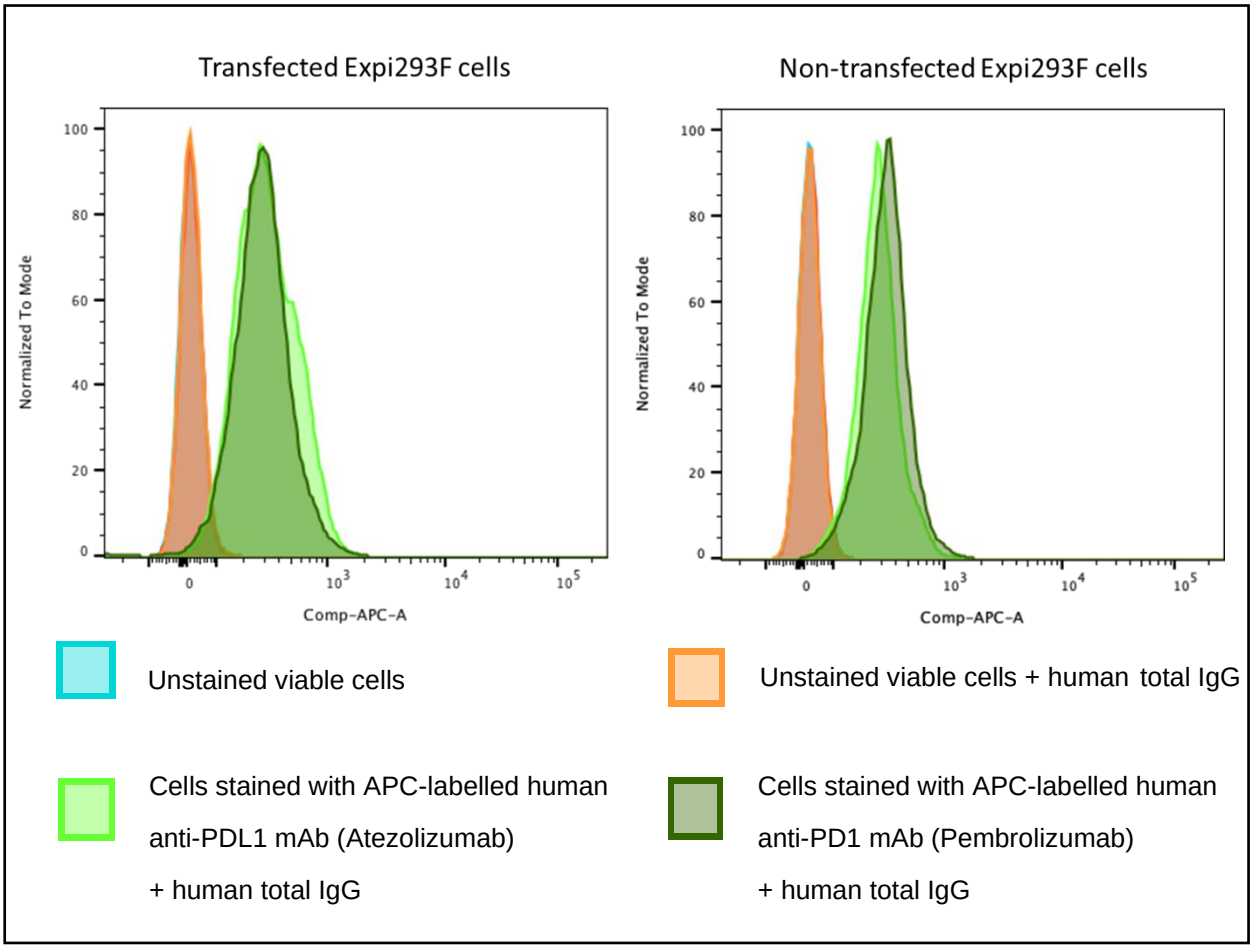

figure 30: Flow cytometric analysis showing the binding affinities of human APC-labeled anti-PD-1 (Pembrolizumab) and anti-PD-L1 (Atezolizumab) mAbs to the human cell line Expi293F used for expression of caninized mAbs with the geometric mean fluorescent intensity (MFI) visualized as graph. Binding capacities of non-transfected as well as transfected cells, expressing mAb-Pembro-IgG1 were tested.

table 18: Results from flow cytometric analysis showing the binding affinities of human APC-labeled anti-PD-1 and anti-PD-L1 mAbs to non-transfected as well as transfected Expi293F cells evaluated by determination of MFI APC values.

	MFI APC	
	Non-transfected Expi293F cells	Transfected Expi293F cells
Unstained viable cells	34	25
Unstained viable cells + human total IgG	31	27
Cells stained with APC-labelled human anti-PDL1 mAb (Atezolizumab) + human total IgG	288	322
Cells stained with APC-labelled human anti-PD1 mAb (Pembrolizumab) + human total IgG	335	292

Flow cytometric analysis resulted in significant increase of APC signal detected for all samples stained with labelled human mAbs, considering values of ≥150 MFI (APC) as significant. These results suggest that Expi293F cells express both checkpoint molecules on their surface. In non-transfected Expi293F cells, human anti-PD-1 has a slightly higher binding affinity. Interestingly, cells transfected with pVITRO-Pembro-IgG1 resulted in slightly higher binding affinities of human anti-PD-L1 Atezolizumab, with MFI (APC)= 322, while staining with anti-PD-1 Pembrolizumab lead to a lower value of 292. These results correlate with the hypothesis that Expi293F cells express both checkpoint molecules on the cell surface, leading to binding of produced caninized mAbs to PD-1 or PD-L1. Binding of caninized mAbs to cell surface molecules might further interfere with the binding of human mAbs, leading to reduced fluorescent signals. Further investigations are suggested to ensure that detected APC-signals resulted from specific binding of human anti-PD-1 and anti-PD-L1 to PD-1 and PD-L1 on the surface of cells.

5. Conclusion

This master thesis project aimed to establish a convenient, cost- and time-efficient process to produce caninized anti-PD-1 as well as anti-PD-L1 mAbs, equipped with specific canine constant IgG1 or IgG4 regions, as well as variable sequences of the human ICIs Pembrolizumab (anti-PD-1) or Atezolizumab (anti-PD-L1). The human Expi293F cell line was used as expression system and was transfected in suspension as well as under adherent conditions. Application of adherent conditions is more time-consuming, taking up to one month until purification and results concerning antibody yield need to be further evaluated and compared to transfection in suspension in future studies. However, the technique is convenient for selection of positive cell clones using hygromycin B. Our results further suggested that positive clones were easily frozen and thawed again, with plasmids remaining incorporated. Transfection of cells in suspension was more time-efficient, taking only one week until purification of antibodies. All mAb isotypes were detected in the supernatant of transfected cells in suspension at different concentrations, after one week of growth, revealed via dot blots. Antibodies were further detected in purified fractions following affinity chromatography using dot blots. However, caninized IgG1 anti-PD-L1 mAb was the only antibody showing a correct molecular mass under both reducing as well as non-reducing conditions, as revealed via SDS-PAGE and western blots after purification via affinity chromatography. For detection of mAbs on dot blots as well as western blots, an HRP conjugated anti-dog IgG antibody from rabbit origin was used, targeting the Fc domain of canine antibody heavy chains. A consideration to take into account was that antibodies were to a certain extent trapped on or in the expression cell line Expi293F. This assumption was confirmed by results from dot blots and is a slight drawback of the expression method, which should be optimized in future studies. The antibody concentration was tested using samples from the cell supernatant and cell pellets after each centrifugation step, performed for removal of cell components before affinity chromatography. Antibody concentration in the supernatant was reduced substantially after the first centrifugation step, and mAbs could be detected within the cell pellets. We hypothesized that the observed antibody loss from the supernatant might result from the binding of caninized mAbs to the surface of Expi293F cells. Therefore, we next determined whether these cells express the checkpoint molecules PD-1 or PD-L1. We labeled human anti-PD-1 Pembrolizumab and anti-PD-L1 Atezolizumab with APC and tested the binding affinities to non-transfected as well as transfected Expi293F cells. Flow cytometric analyses revealed that human anti-PD-1 as well as anti-PD-L1 mAbs possessed significant binding capacities to the human expression cell line, further showing that binding capacity is reduced in transfected cells for the same antibody isotype. We consider that binding of caninized mAbs via the surface of cells might lead to downregulation of protein synthesis, considering the inhibitory properties of checkpoint molecules PD-1 and its ligand PD-L1. Following further

analysis, the use of another expression cell line might be considered for future studies, suggesting Chinese hamster ovary (CHO) cells. This cell line also exists as improved expression cell line (ExpiCHO™ cells, Thermo Fisher Scientific) for production of high yields of protein. Another finding achieved via flow cytometric analysis was that human anti-PD-1 Pembrolizumab and anti-PD-L1 Atezolizumab exhibit significant binding affinities to the canine mammary carcinoma cell lines CF33, CF41 and canine osteosarcoma cell line D-17, suggesting that the tested canine cancer cell lines express the checkpoint molecules PD-1 and PD-L1 on their surface, similarly to what was already demonstrated for the macrophage-like canine cancer cell line DH82 in preliminary results from our lab. Our results suggest that caninized mAbs may be used for treatment of these tumour types, canine mammary cancer and osteosarcoma, and maybe others in the future. Major improvements were further achieved in this master thesis project in the production of higher DNA plasmid yields testing different cultivation conditions of recombinant *E. coli* cells. Plasmid DNA sequences were evaluated by DNA sequencing and alignment analyses showed correlation to reference sequences. Further, we were able to reduce costs for the cultivation of Expi293F cells, testing growth conditions in a different medium. The SFM4HEK293 medium was shown to provide similar culture conditions for the human Expi293F cell line, leading to ≥90 % cell viability. Overall, the results from this study add major advancements towards the establishment of ICI-based immunotherapy against multiple dog cancers via caninized anti-PD-1 and anti-PD-L1 mAbs with specific canine IgG1 or IgG4 regions.

6. References

Abbott, M., Ustoyev, Y. (2019) *Cancer and the Immune System: The History and Background of Immunotherapy.* Seminars in Oncology Nursing. 35. 150923.

Adams, V.J., Evans, K.M., Sampson, J., Wood, J.L.N. (2010) *Methods and mortality results of a health survey of purebred dogs in the UK.* Journal of Small Animal Practice. 51, 512–524.

Ai, L., Xu, A., Xu, J., (2020) *Roles of PD-1/PD-L1 Pathway: Signaling, Cancer, and Beyond.* Advances in Experimental Medicine and Biology. 1248, 33-59.

Amin, S.B., Anderson, K.J., Boudreau, C.E., Martinez-Ledesma, E., Kocakavuk, E., Johnson, K.C., Barthel, F.P., Varn, F.S., Kassab, C., Ling, X., Kim, H., Barter, M., Lau, C.C., Ngan, C.Y., Chapman, M., Koehler, J.W., Long, J.P., Miller, A.D., Miller, C.R., Porter, B.F., Rissi, D.R., Mazcko, C., LeBlanc, A.K., Dickinson, P.J., Packer, R.A., Taylor, A.R., Rossmeisl, J.H., Woolard, K.D., Heimberger, A.B., Levine, J.M., Verhaak, R.G.W. (2020) *Comparative Molecular Life History of Spontaneous Canine and Human Gliomas*. Cancer Cell. 37(2); 243-257.e7.

Boo, G., Leyk, S., Fabrikant, S.I., Graf, R., Pospischil, A., (2019) *Exploring Uncertainty in Canine Cancer Data Sources Through Dasymetric Refinement.* Frontiers in Veterinary Science. 6, 45.

Brom, V.C., Burger, C., Wirtz, D.C., Schildberg, F.A., (2022) *The Role of Immune Checkpoint Molecules on Macrophages in Cancer, Infection, and Autoimmune Pathologies.*Frontiers in Immunology. 13, 837645

Butte, M.J., Keir, M.E., Phamduy, T.B., Sharpe, A.H., Freeman, G.J. (2007) *Programmed Death-1 Ligand 1 Interacts Specifically with the B7-1 Costimulatory Molecule to Inhibit T Cell Responses.* Immunity. 27 111–122.

Choi, J.W., Withers, S.S., Chang, H., Spanier, J.A., de La Trinidad, V.L., Panesar, H., Fife, B.T., Sciammas, R., Sparger, E.E., Moore, P.F., Kent, M.S., Rebhun, R.B., McSorley, S.J., (2020) Development of canine PD-1/PD-L1 specific monoclonal antibodies and amplification of canine T cell function. PLOS ONE. 15 (7): e0235518.

Dillekås, H., Rogers, M.S., Straume, O., (2019). *Are 90% of deaths from cancer caused by metastases?* Cancer Medicine. 8, 5574–5576.

Eno, J., (2017) *Immunotherapy through the years.* Journal of the Advanced Practitioner in Oncology. 8.747-753.

EMA (2022) *Keytruda.* European Medicines Agency, accessed 10 July 2022, <https://www.ema.europa.eu/en/medicines/human/EPAR/keytruda>

EMA (2022) *Tecentriq.* European Medicines Agency, accessed 10 July 2022, <https://www.ema.europa.eu/en/medicines/human/EPAR/tecentriq>

Gardner, H.L., Fenger, J.M., London, C.A., (2016) *Dogs as a model for cancer.* Annual Review of Animal Biosciences. 4, 199-222.

GE Healthcare (2009) *HiTrap Protein A HP, HiTrap affinity columns.* Product Information Sheet. 71-7002-00 AP

Glikin, G.C., Finocchiaro, L.M.E., (2014) *Clinical Trials of Immunogene Therapy for Spontaneous Tumors in Companion Animals*. The Scientific World Journal. 718520.

Gonzalez, H., Hagerling, C., Werb, Z., (2018) *Roles of the immune system in cancer: from tumor initiation to metastatic progression*. Genes & Development. 32, 1267-1284.

Han, Y., Liu, D., Li, L., (2020) *PD-1/PD-L1 pathway: current researches in cancer.* The American Journal of Cancer Research. 10(3), 727-742

Hanahan, D., (2022) *Hallmarks of Cancer: New Dimensions*. Cancer Discovery. 12, 31-46

Hanahan, D., Weinberg, R.A., (2011) *Hallmarks of cancer: The next generation*. Cell. 144.

Hulvat, M.C., (2020) *Cancer Incidence and Trends*. Surgical Clinics of North America. 100, 3. 469-481.

Igase, M., Nemoto, Y., Itamoto, K., Tani, K., Nakaichi, M., Sakurai, M., Sakai, Y., Noguchi, S., Kato, M., Tsukui, T., Mizuno, T., (2020) *A pilot clinical study of the therapeutic antibody against canine PD-1 for advanced spontaneous cancers in dogs*. Scientific Reports. Nature Research. 10, 18311

IGTM database (2022) *The International Immunogenetics information system* accessed 10 July 2022, <https://www.imgt.org/>

Jiang, Y., Chen, M., Nie, H., Yuan, Y., (2019) *PD-1 and PD-L1 in cancer immunotherapy: clinical implications and future considerations.* Human Vaccines and Immunotherapeutics. 15, 5, 1111–1122.

Kennedy, L.B., Salama, A.K.S., (2020) *A Review of Cancer Immunotherapy Toxicity*. Cancer Journal for Clinicians 70, 86–104.

Killick, D.R., Stell, A.J., Catchpole, B., (2015) *Immunotherapy for canine cancer - Is it time to go back to the future?* Journal of Small Animal Practice. 56, 229-241

Kim, S.K., Cho, S.W., (2022) *The Evasion Mechanisms of Cancer Immunity and Drug Intervention in the Tumor Microenvironment.* Frontiers in Pharmacology 13. 868695.

Kirley, T.L., Norman, A.B., (2018) *Biochemical and Biophysical Research Communications.* Biochemical and Biophysical Research Communications 1-6. 503, 944–949.

Klingemann, H., (2018) *Immunotherapy for dogs: Running behind humans*. Frontiers in Immunology. 9, 133

Klingemann, H., (2021) *Immunotherapy for Dogs: Still Running Behind Humans.* Frontiers in Immunology. 12, 665784

Lessard, J.C., (2013) *Growth media for E. coli.* Methods in Enzymology. 533, 181–189.

MacWilliams, M.P., Liao, M.-K., (2016*) Luria Broth (LB) and Luria Agar (LA) Media and Their Uses Protocol.* American Society for Microbiology.

Maekawa, N., Konnai, S., Ikebuchi, R., Okagawa, T., Adachi, M., Takagi, S., Kagawa, Y., Nakajima, C., Suzuki, Y., Murata, S., Ohashi, K., (2014) *Expression of PD-L1 on Canine Tumor Cells andEnhancement of IFN-cProduction from Tumor-Infiltrating Cells by PD-L1 Blockade.* PLOS ONE 9, 6, e98415

Maekawa, N., Konnai, S., Okagawa, T., Nishimori, A., Ikebuchi, R., Izumi, Y., Takagi, S., Kagawa, Y., Nakajima, C., Suzuki, Y., Kato, Y., Murata, S., Ohashi, K., (2016) *Immunohistochemical Analysis of PD-L1 Expression in Canine Malignant Cancers and PD-1 Expression on Lymphocytes in Canine Oral Melanoma.* PLOS ONE 11. 11(6): e0157176

Muenst, S., Läubli, H., Soysal, S.D., Zippelius, A., Tzankov, A., Hoeller, S., 2016. The immune system and cancer evasion strategies: Therapeutic concepts. Journal of Internal Medicine. 279, 541–562

Okonechnikov, K., Golosova, O., Fursov, M., Varlamov, A., Vaskin, Y., Efremov, I., German Grehov, O.G., Kandrov, D., Rasputin, K., Syabro, M., Tleukenov, T., (2012) *Unipro UGENE: A unified bioinformatics toolkit.* Bioinformatics. 28, 8, 1166–1167.

Pérez-Herrero, E., Fernández-Medarde, A., (2015) *Advanced targeted therapies in cancer: Drug nanocarriers, the future of chemotherapy*. European Journal of Pharmaceutics and Biopharmaceutics. 0939-6411.

Plesca, I., Tunger, A., Müller, L., Wehner, R., Lai, X., Grimm, M.O., Rutella, S., Bachmann, M., Schmitz, M., (2020) *Characteristics of Tumor-Infiltrating Lymphocytes Prior to and During Immune Checkpoint Inhibitor Therapy*. Frontiers in Immunology. 11, 364.

Raybould, M.I.J., Marks, C., Lewis, A.P., Shi, J., Bujotzek, A., Taddese, B., Deane, C.M., (2020) *Thera-SAbDab: the Therapeutic Structural Antibody Database.* Nucleic Acids Research 48, D383–D388.

Sanghera, C., Sanghera, R., (2019) *Immunotherapy – Strategies for Expanding Its Role in the Treatment of All Major Tumor Sites.* Cureus. 11(10): e5938.

Schiffman, J.D., Breen, M., (2015) *Comparative oncology: What dogs and other species can teach us about humans with cancer*. Phil. Trans. R. Soc. B. 370: 20140231.

Schreiber, R.D., Old, L.J., Smyth, M.J., (2011) *Cancer Immunoediting: Integrating Immunity's Roles in Cancer Suppression and Promotion.* Science. 331. 1565-1570.

Seyfried, T.N., Huysentruyt, L.C., (2013) *On the Origin of Cancer Metastasis.* Critical Reviwes in Oncology. 8(1-2): 43–73

Sigma-Aldrich (2015), *GenElute Plasmid Midiprep Kit*. Product Information Sheet. PLD35

Stevenson, V.B., Perry, S.N., Todd, M., Huckle, W.R., LeRoith, T., (2021) *PD-1, PD-L1, and PD-L2 Gene Expression and Tumor Infiltrating Lymphocytes in Canine Melanoma.* Veterinary Pathology. 58, 692–698.

Sung, H., Ferlay, J., Siegel, R.L., Laversanne, M., Soerjomataram, I., Jemal, A., Bray, F., (2021) *Global Cancer Statistics 2020: GLOBOCAN Estimates of Incidence and Mortality Worldwide for 36 Cancers in 185 Countries.* CA: A Cancer Journal for Clinicians. 71. 3, 209- 249

Thermo Fisher Scientific (2019) *Expi293F™ cell lines.* Gibco Product Information Sheet. MAN0006283.

Wang, W., Li, W., Chu, D., Hua, J., Zhang, X., Lu, D., Wang, Y., Zhang, S., (2021) *Long-term assessment of risk factors for canine tumors registered in Xi'an, China.* Animal Diseases. 1, 30.

Wei, F., Wang, D., Wei, J., Tang, N., Tang, L., Xiong, F., Guo, C., Zhou, M., Li, X., Li, G., Xiong, W., Zhang, S., Zeng, Z., (2021) *Metabolic crosstalk in the tumor microenvironment regulates antitumor immunosuppression and immunotherapy resisitance*. Cellular and Molecular Life Sciences. 78, 173–193.

WHO (2022) *Cancer.* World Health Organization, accessed 10 July 2022, <https://www.who.int/news-room/fact-sheets/detail/cancer>

Yeo, M.K., Choi, S.Y., Seong, I.O., Suh, K.S., Kim, J.M., Kim, K.H., (2017) *Association of PD-L1 expression and PD-L1 gene polymorphism with poor prognosis in lung adenocarcinoma and squamous cell carcinoma.* Human Pathology. 68, 103–111.

Zhang, Y., Zhen, J., (2020) *Functions of Immune Checkpoint Molecules Beyond Immune Evasion.* Advances in Experimental Medicine and Biology. 1248, 201-226.

Zuleger, C.L., Kang, C., Ranheim, E.A., Kurzman, I.D., Macklin, M.D., Newton, M.A., Wolchok, J.D., Vail, D.M., Eriksson, E., Albertini, M.R., (2017) *Pilot study of safety and feasibility of DNA microseeding for treatment of spontaneous canine melanoma*. Veterinary Medicine and Science. 3, 134–145.

7. List of figures

8. List of tables

9. Appendix

9.1. Materials Preliminary data: Plasmid production

- Q5 Mastermix: Q5® High-Fidelity 2X Mastermix (#M0492S, New England Biolabs)
- PCR Thermocycler: TProfessional BASIC 96 Gradient (Biometra)
- pVITRO1-hygro-mcs plasmid (#pvitro1-mcs, Invitrogen)
- DNA purification kit: Wizard® SV Gel and PCR Clean-Up System (#A9281; Promega)
- Spectrophotometer: NanoPhotometer Pearl (Implen)
- Chemically competent *E. coli* cells: NEB® 10-beta Competent *E. coli* (#C3019H, New England Biolabs)
- Hygromycin B Selection Agar Plates:
  - 15 g Agar
  - 1 µl Hygromycin B (#1287.2, Carl Roth)
  - 5 g NaCl
  - 10 g Pepton
  - 5 g Yeast Extract
  - MiliQ H2O ad. 1 L
- Incubator: New Brunswick™ Innova ®42/42R Shaker (Eppendorf)
- Outgrowth Medium: NEB 10-beta/Stable Outgrowth Medium (#B9035, New England Biolabs)
- Plasmid Miniprep System: PureYield™ Plasmid Miniprep System (#A1222, Promega)

table 19: Primers used for amplification and generation of overlapping DNA fragments via PCR; All primers are used at concentrations of 10 µM.

Primer name	DNA sequence (5'-3')	Tm (°C)
Atezo_VH_fwd	44 bp; GCGGCCGC …… GTGGAGAG	98.2
Atezo_VL_fwd	47 bp; TGGGTTCC …… AGCCCCAG	93.2
canG1_rev	38 bp; GTCTGGCC …… CGGAGAAT	79.3
can_kappa_rev	41 bp; AGGCGTAC …… CTGACACT	80.6
F2_IgG1_IgG4_CH_FW	30 bp; AACTGTGT …… TCCTTGAC	77.8
F2_IgG1_IgG4_CH_REV	30 bp; GGGTCTGA …… AAAACTCA	78.2
F4_Pem_Ate_VH_FWD	30 bp; CGGAATTC …… AGGCTCGG	78.6
F4_Pem_Ate_VH_REV	30 bp; TTCTGGCT …… GAGACCCT	76.5
hph_EF1pAn_Rev	42 bp; ATCTAGCT …… TGTGGAGG	78.6
IRES_fwd	38 bp; TGATAGGG …… TTTCCCCA	84.6

Pembro_VH _fwd	42 bp; GGCCGCCA …… GTGCAGAG	97
Pembro_VL_fwd	42 bp; TGGGTTCC …… CCCAGAGC	91.2
pVitro_H_lead_rev	40 bp; GGAGTGCG …… AGAGGATC	94
pVitro_L_lead_rev	40 bp; ACCGCGGC …… ATGAGTTG	89.1
SV40_fwd	41 bp; TGTACAGC …… ATTGATGA	77.6

9.2. Methods Preliminary data: Plasmid production

Preliminary data was produced in the context of two laboratory courses, namely “Wahlbeispiel 1” and “Großpraktikum”, which were undertaken at the Department of Comparative Medicine at the Interuniversity Messerli Research Institute within the current project. Plasmids were first constructed in silico, using the software UGENE (Okonechnikov et al., 2012), and assembled via MOE-PCR, a ligation independent cloning technique. Further, competent *E. coli* cells were transformed and cultured on hygromycin B selection agar plates and plasmids were isolated using a Plasmid Miniprep system. In the following text, plasmids are referred to as “pVITRO-Atezo-IgG1”, “pVITRO-Atezo-IgG4”, “pVITRO-Pembro-IgG1” and “pVITRO-Pembro-IgG4, whereat “Atezo” is the short form of Atezolizumab (human anti-PD-L1 mAb) and “Pembro” refers to Pembrolizumab (human anti-PD-1 mAb).

9.2.1. In silico construction of plasmid via the software UGENE

For digital construction of plasmids, the software UGENE was used. The pVITRO1-hygro-msc plasmid was used as backbone, possessing a variety of convenient features *(figure 9)*. The vector carries two elongation factor 1 alpha (EF-1α) promoters, from mouse and rat origin, as well as two enhancer genes, Simian virus 40 (SV40) and cytomegalovirus (CMV) enhancer, which are located upstream of each one promoter. This allows for simultaneous expression as well as enhancement of gene expression of two genes, in this case antibody heavy as well as light chain.

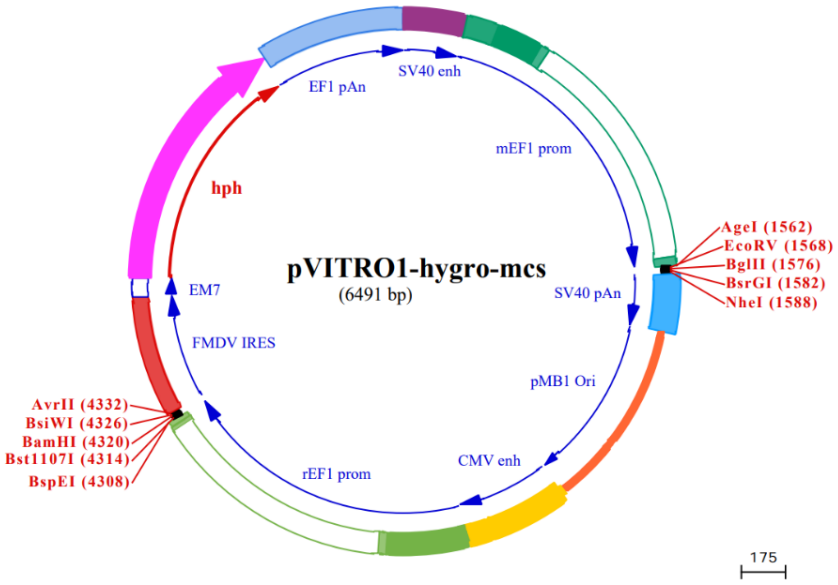

figure 31: Vector pVITRO1-hygro-mcs provides 2 MCS for convenient integration of inserts and allows for simultaneous expression of two genes; **CMV enh:** cytomegalovirus enhancer, **EF1 pAn:** Elongation factor 1 polyadenylation signal, **EM7:** synthetic promoter allowing constitutive expression derived from *E. coli* T7 promoter, **FMDV IRES:** Foot and Mouth Disease internal ribosome entry site, **hph:** hygromycin resistance gene, **mEF1 prom:** elongation factor 1 alpha promoter from mouse origin, **pMBI Ori:** minimal *E. coli* origin of replication, **rEF1 prom:** elongation factor 1 alpha promoter from rat origin, **SV40 enh:** Simian virus 40 enhancer, **SV40pAn:** Simian Virus 40 late polyadenylation signal

Furthermore, the pVITRO1-hygro-msc plasmid contains two multiple cloning sites, MSC 1 and MSC 2, each located downstream of one EF-1α promoter. Each MSC incorporates several restriction sites, facilitating insertion of desired sequences. The plasmid was constructed in a way that the variable and constant light chain sequences are located downstream of the rat origin EF-1α promoter (rEF 1 prom) and are thus under its transcriptional control, while the variable and constant heavy chain regions are located downstream of and expressed from the mouse origin EF-1α promoter (mEF 1 prom). Sequences of human therapeutic anti-PD-1 (Pembrolizumab) and anti-PD-L1 (Atezolizumab) representing variable heavy and light chain regions were obtained from The Therapeutic Structural Antibody Database (Raybould et al., 2020). Constant heavy and kappa light chain sequences of canine IgG1 or IgG4 were obtained from the IMGT database (IMGT, 2022). The pVITRO1-hygro-msc vector contains an antibiotic resistance gene (hph gene), conferring resistance to hygromycin B both in *E. coli* and mammalian cells. The EM7 promoter enables constitutive expression of the hph gene in E. coli, while in eukaryotic cells, the gene is expressed from the rat EF-1α promoter. For replication in *E. coli* cells, a minimal *E. coli* origin of replication (pMB1 ori) is incorporated, while the internal ribosome entry site of the Foot and Mouth Disease Virus (FMDV IRES) enables the translation of two open reading frames from one mRNA in eukaryotic cells. SV40 late polyadenylation signal (pAn) and EF1 pAn serve for efficient cleavage of mRNA.

9.2.2. Production of overlapping DNA fragments

For assembly of each plasmid, 4 DNA fragments were produced and amplified via PCR, creating 21 bp of overlapping regions between adjacent DNA fragments. The applied PCR conditions, template DNA and primers are summarized in the following. All the PCR runs were conducted with 1 ng of template DNA, 25 µl Q5 Mastermix and ultrapure water up to a final volume of 50 µl. Primers were added to a final concentration of 0.5 µM per reaction. The pVitro1 plasmid backbone used as template was obtained by previous pVitro1 clones produced in our lab. The other DNA templates were obtained by BioCat GmbH, including plasmids carrying the heavy chain sequence of Atezolizumab in frame with the sequence of canine IgG1, the heavy chain sequence of Pembrolizumab in frame with the sequence of canine IgG4, the light chain sequence of Atezolizumab in frame with the sequence of canine Kappa constant chain and the light chain sequence of Pembrolizumab in frame with the sequence of canine Kappa constant chain. The other two plasmid isotypes were generated in a subsequent step, using the produced plasmids as template. Tables 20, 21, 23 and 24 provide an overview of the used template DNA and primer pairs, while the PCR conditions are summarized in tables 22, 25 and 26.

table 20: Template DNA and primer pairs used for amplification of DNA fragments 1- 4 for assembly of the plasmid pVITRO-Atezo-IgG1 via PCR

DNA fragment	Template DNA	Forward primer	Reverse primer
1	Atezo_VL_IgKL pUC57	Atezo_VL_fwd	can_kappa_rev
2	Atezo_VH_IgG1 pUC57	Atezo_VH_fwd	canG1_rev
3	pVITRO1-hygro-mcs-hu225_IgE_kappa_VKK_new	SV40_fwd	pVitro_L_lead_rev
4	pVITRO1-hygro-mcs-hu225_IgE_kappa_VKK_new	IRES_fwd	pVitro_H_lead_rev

table 21: Template DNA and primer pairs used for amplification of DNA fragments 1- 4 of the plasmid pVITRO-Pembro-IgG4 via PCR

DNA fragment	Template DNA	Forward primer	Reverse primer
1	Pemb_VL_IgKL pUC57	Pemb_VL_fwd	can_kappa_rev
2	Pemb_VH_IgG4 pUC57	Pemb_VH_fwd	canG1_rev
3	pVITRO1-hygro-mcs-hu225_IgE_kappa_VKK_new	SV40_fwd	pVitro_L_lead_rev
4	pVITRO1-hygro-mcs-hu225_IgE_kappa_VKK_new	IRES_fwd	pVitro_H_lead_rev

table 22: PCR amplification of overlapping DNA fragments for the assembly of plasmids pVITRO-Atezo-IgG1 and pVITRO-Pembro-IgG4; F1-4: DNA fragments 1-4

Step	T (°C)				Time (s)				Repeats
DNA fragments	F1	F2	F3	F4	F1	F2	F3	F4	
Initial denaturation	98				30				
Denaturation	98				10				20
Annealing	62		65		30				
Extension	72				25	35	98		
Final Extension	72				120				
Hold	4				∞				

table 23: Template DNA and primer pairs used to produce DNA fragments 1-4 of pVITRO-Atezo-IgG4 via PCR

DNA fragment	Template DNA	Forward primer	Reverse primer
1	pVITRO-hygro-Atezo-IgG1	Atezo_VL_fwd	hph_EF1pAn_Rev
2	pVITRO-hygro-Pembro-IgG4	F2_IgG1_IgG4_CH_FW	F2_IgG1_IgG4_CH_REV
3	pVITRO-hygro-Atezo-IgG1	SV40_fwd	pVitro_L_lead_rev
4	pVITRO-hygro-Atezo-IgG1	F4_Pem_Ate_VH_FWD	F4_Pem_Ate_VH_REV

table 24: Template DNA and primers used for the amplification of DNA fragments 1-4 of pVITRO-Pembro-IgG1 via PCR

DNA fragment	Template DNA	Forward primer	Reverse primer
1	pVITRO-hygro-Pembro-IgG4	Pemb_VL_fwd	hph_EF1pAn_Rev
2	pVITRO-hygro-Atezo-IgG1	F2_IgG1_IgG4_CH_FW	F2_IgG1_IgG4_CH_REV
3	pVITRO-hygro-Pembro-IgG4	SV40_fwd	pVitro_L_lead_rev
4	pVITRO-hygro-Pembro-IgG4	F4_Pem_Ate_VH_FWD	F4_Pem_Ate_VH_REV

table 25: PCR amplification of DNA fragments 2- 4 of plasmids pVITRO-Pembro-IgG1 and pVITRO-Atezo-IgG4. For amplification of DNA fragment 3: 20 cycles and for DNA fragments 2 and 4: 25 cycles of Denaturation, Annealing and Extension; F1-4: DNA fragments 1-4

Step	T (°C)			Time (s)			Repeat
DNA fragments	F3	F2	F4	F3	F2	F4	
Initial denaturation	98			30			
Denaturation	98			10			20/ 25
Annealing	65	64		30			
Extension	72			98	90		
Final Extension	72			120			
Hold	4			∞			

table 26: PCR amplification of DNA fragment 1 of plasmids pVITRO-Pembro-IgG1 and pVITRO-Atezo-IgG4

Step	T (°C)	Time (s)	Repeats
Initial denaturation	98	60	
Denaturation	98	30	
Annealing			30
Extension	72	120	
Final Extension	72	120	
Hold	4	∞	

9.2.3. Purification of overlapping DNA fragments

Amplified DNA fragments were separated by electrophoresis on an agarose gel (*see Methods 4.2.1.)* Following electrophoresis, DNA bands were excised from the agarose gel and placed in 1.5 ml microcentrifuge tubes. Membrane Binding Solution was added in an equal volume (µl) to the weight (mg) of the gel slices. The tubes were vortexed and incubated at 50–65 °C until the gel slices were completely dissolved. Next, minicolumns were inserted into collection tubes. Dissolved gel mixtures were transferred to collection tubes and incubated at room temperature (RT) for one minute. Next, tubes were centrifuged (16,000 × g, 1 minute, RT). The flowthrough was discarded and minicolumns were reinserted into collection tubes. Then, 700 µl Membrane Wash Solution were applied to the columns and the tubes were again centrifuged (16,000 × g, 1 min, RT). The flowthrough was discarded and minicolumns were reinserted into the collection tubes. Another 500 µl Membrane Wash Solution were added and tubes were centrifuged (16,000 × g, 5 min, RT). After discarding the flowthrough and reinserting the

columns, tubes were centrifuged (20 000 x g, 1 min, RT) with the microcentrifuge lid open to allow evaporation of any residual ethanol. The minicolumns were then transferred to clean 1.5 ml microcentrifuge tubes. For elution, 25 µl of 10 µM TRIS-HCl were applied to the minicolumns and the tubes were incubated at RT for one minute. Tubes were centrifuged (16,000 × g, 1 min, RT). Minicolumns were discarded and purified DNA was stored at 4 °C or –20 °C. Following isolation of DNA fragments, DNA concentrations were measured using a spectrophotometer at a wavelength of 260 nm.

9.2.4. Plasmid assembly via Ligation Independent Cloning: MOE- PCR

For assembly via MOE-PCR, DNA fragments were mixed according to values calculated via formula 1. The largest DNA fragment 4 served as vector backbone, while fragments 1, 2 and 3 were considered as inserts with a molar ratio of 1:1 between fragment 3 and 4, and a molar ratio of 1: 2 between fragment 1 and 2 with the vector backbone, taking into consideration the length of each DNA fragment in bp. An amount of 100 ng of vector backbone was used.

$$m\,(insert) = \frac{insert}{vector} molar\ ratio * m\,(vector) * \frac{insert\ length}{vector\ lenth}$$

formula 1

Overlapping DNA fragments were assembled in one step in vitro via a specific touchdown PCR program *(table 27),* whereat fragments served as templates as well as primers for each other. The PCR reaction was performed adding the calculated volumes of each DNA fragment, 25 µl of Q5 Mastermix and ultrapure water to a final volume of 50 µl.

table 27: PCR conditions for the assembly of DNA plasmids; MOE-PCR works by a specific touchdown program, whereat the annealing temperature is gradually decreased, aimed at increasing the specificity of binding

Step	T (°C)	Time (s)	∆ T (°C)	Repeats
Initial denaturation	98	30		
Touchdown step	98	10	-0.5	14
	75	20		
	72	225		
Denaturation	98	10		15
Annealing	68	20		
Extension	72	225		
Final Extension	72	5 min		
Hold	4	∞		

9.2.5. Transformation of *E. coli* and plasmid purification

For each transformation reaction, one tube of chemically competent *E. coli* cells was thawed on ice for 10 minutes. Next, 5 µl containing 1 pg- 100 ng of plasmid DNA were added to the cells, flicking tubes carefully to mix DNA and cells. Cell mixtures were placed on ice for 30 minutes, followed by a heat-shock at 42 °C for 30 seconds. The tubes were placed on ice again for 5 minutes and subsequently, 950 µl of Outgrowth Medium were added to the mixture. Tubes were then placed in a thermoshaker (37 °C, 60 min, 350 rpm). In the meantime, hygromycin selection plates, containing 50 µg/ml of hygromycin B, were incubated at 37 °C. Finally, 80 µl of each transformation mixture were spread on hygromycin selection plates and incubated overnight at 37 °C. The next day, one colony of each plasmid isotype was transferred to each 3 ml of liquid low salt LB media and incubated at 37 °C and 250 rpm overnight. For purification of plasmid DNAs, a Miniprep system was used, as described in Methods 3.1.1.2. For preservation of the obtained plasmids, recombinant *E. coli* cells were kept in glycerol stocks, mixing cells and 50 % glycerol 1:1 and stored at -80 °C.